

**This is an ACCEPTED VERSION of the following published document:**

D. Pérez-Adán, M. Joham, Ó. Fresnedo, J. P. González-Coma, L. Castedo and W. Utschick, “Alternating Minimization for Wideband Multiuser IRS-Aided MIMO Systems Under Imperfect CSI”, *IEEE Transactions on Signal Processing*, vol. 72, pp. 99-114, 2024, doi: 10.1109/TSP.2023.3336166.

Link to published version: <https://doi.org/10.1109/TSP.2023.3336166>

**General rights:**

©2023 IEEE. This version of the article has been accepted for publication, after peer review. Personal use of this material is permitted. Permission from IEEE must be obtained for all other uses, in any current or future media, including reprinting/republishing this material for advertising or promotional purposes, creating new collective works, for resale or redistribution to servers or lists, or reuse of any copyrighted component of this work in other works.

# Alternating Minimization for Wideband Multiuser IRS-aided MIMO Systems under Imperfect CSI

Darian Pérez-Adán, *Member, IEEE*, Michael Joham, *Member, IEEE*, Óscar Fresnedo, *Member, IEEE*, José P. González-Coma, Luis Castedo, *Senior Member, IEEE* and Wolfgang Utschick, *Fellow Member, IEEE*

**Abstract**—This work focuses on wideband intelligent reflecting surface (IRS)-aided multiuser MIMO systems. One of the major challenges of this scenario is the joint design of the frequency-dependent base station (BS) precoder and user filters, and the IRS phase-shift matrix which is frequency flat and common to all the users. In addition, we consider that the channel state information (CSI) is imperfect at both the transmitter and the receivers. A statistical model for the imperfect CSI is developed and exploited for the system design. A minimum mean square error (MMSE) approach is followed to determine the IRS phase-shift matrix, the transmit precoders, and the receiving filters. The broadcast (BC)-multiple access channel (MAC) duality is used to solve the optimization problem following an alternating minimization approach. Numerical results show that the proposed approach leads to substantial performance gains with respect to baseline strategies that neglect the inter-user interference and do not optimize the IRS phase-shift matrix. Further performance gains are obtained when incorporating into the system design the statistical information of the channel estimation errors.

**Index Terms**—Downlink, mmWave, IRSs, wideband, BC-MAC duality, imperfect CSI, multiuser, multistream.

## I. INTRODUCTION

**A**N intelligent reflecting surface (IRS) is a metasurface comprising a multitude of low-cost passive reflective elements whose response can be configured in real-time [1–6]. IRSs are attracting significant attention as a key enabling technology for multiple-input multiple-output (MIMO) systems to reach the capacity requirements demanded by the next generations of wireless communication systems [7–11].

The IRS technology offers tremendous benefits for various application scenarios [12]. In device-to-device (D2D) networks [13], IRSs can be utilized to cancel interference, support low-power transmission, and enhance individual data links. In cognitive radio (CR) networks, the IRSs play a crucial role in increasing the degrees of freedom and improving the efficiency of secondary transmissions [14, 15]. Another interesting application of IRSs is in cellular network systems with cell edge users. These users often suffer from high signal attenuation from the BS and co-channel interference from nearby BSs. By deploying IRSs in such scenarios, the

coverage area in the cellular network can be expanded as IRSs efficiently reflect the signal from the BS to the cell edge user, compensating for signal attenuation and interference, as demonstrated in [16]. Moreover, IRSs find intriguing applications in unmanned aerial vehicle (UAV) networks. Integrating IRSs in UAV networks can significantly enhance communication quality between UAVs and ground users. This enhancement becomes crucial for optimizing both UAV trajectories and overall system performance, as noted in [17].

Different IRS-aided wireless communication systems have been considered in the literature. In [18], a single-user single-input single-output (SISO) system with a direct channel between both communication ends is considered. In this specific case, the optimal IRS phase-shift matrix is the one that aligns the reflected rays to the direct path between the transmitter and the receiver. However, this solution is not applicable to multiuser (MU) MIMO systems where a common IRS response must be designed for all users.

In [19], the rank improvement of a downlink IRS-aided MIMO system is exploited to obtain capacity gains in a single-user scenario. The authors in [20] have studied the asymptotic achievable rate of the downlink of an IRS-aided MU multiple-input single-output (MISO) system where some users are supported by IRSs while others directly communicate to the BS. The authors propose a modulation scheme that results in achievable sum rates larger than those obtained in non-IRS-aided schemes. In [21], the authors investigate MU MISO downlink communications assisted by a self-sustainable IRS. The reflecting elements of the IRS are classified into two categories: energy harvesting elements and communication elements. As a consequence, the IRS is capable of both reflecting signals and harvesting energy from the received signals. The primary objective of [21] is to maximize the system rate, and to achieve this goal, the authors propose an iterative algorithm that provides a suboptimal solution to the design problem. In [22], an IRS-aided MU non-orthogonal multiple access (NOMA) MISO downlink system—which again enables communication over both the IRS-aided and the direct channels—is addressed. The approach considers the joint optimization of the BS precoders and the IRS phase-shift matrix to minimize the total transmission power. The authors in [23] consider an IRS-aided MU MISO system with an on/off modulation at the reflective elements. In [24], the authors focus on the joint optimization of the IRS phase-shift matrix and the MIMO precoders in an IRS-aided MU MIMO system. Their objective is to maximize the system sum-rate for each channel realization using reinforcement learning strategies.

Darian Pérez-Adán, Óscar Fresnedo and Luis Castedo are with the Department of Computer Engineering, University of A Coruña, CITIC, Spain, e-mail: {d.adan, oscar.fresnedo, luis}@udc.es. José P. González-Coma is with the Defense University Center at the Spanish Naval Academy, jose.gcoma@tud.uvigo.es. Michael Joham and Wolfgang Utschick are with the Department of Electrical and Computer Engineering, Technical University of Munich, Munich, Germany. {joham, utschick}@tum.de

The proposed algorithms are particularly suitable for scenarios with high MU interference. Nevertheless, there are IRS-aided wireless communication use cases that still remain unexplored. For instance, none of the works in [18–23] consider MU MIMO setups, only [24] considers this scheme. They also do not consider wideband transmissions, a relevant feature when communicating through millimeter-wave (mmWave) bands.

Only a few papers have explored the use of IRS-aided systems in wideband scenarios. An example is [25] where an uplink MU single-input multiple-output (SIMO) orthogonal frequency division multiplexing (OFDM) scheme is considered. The focus in [25] is on minimizing the total transmit power by jointly designing the precoders and optimizing the passive beamforming carried out by the IRS.

Wideband systems offer several advantages over conventional narrowband systems, including higher data rates, improved spectral efficiency, and better interference management. Their ability to operate over wider frequency ranges and efficiently utilize wide bandwidths makes them well-suited for modern high-speed communication applications, particularly in scenarios with large data rate demands and multiple users [26].

Employing IRSs in wideband MU systems provides several benefits that can significantly enhance the overall system performance. IRSs can effectively control the propagation environment by intelligently reflecting and redirecting incident signals. This leads to improved signal strength at the receivers, mitigating path loss and signal fading, which is particularly beneficial in wideband scenarios where frequency-selective fading may occur. Additionally, IRSs can be utilized to suppress unwanted interference among users, especially in densely populated MU scenarios. By adjusting the phase shifts of the reflecting elements, the system can actively control signal directions and reduce inter-user interference [6].

In this case of wideband MU systems, the design of IRS-aided wireless systems is challenging because the IRS phase shift matrix is frequency flat while the wireless channels are frequency selective.

Regarding CSI, few works in the literature consider the impact of channel estimation errors when designing robust IRS-aided systems. For instance, in [27], the authors investigate MMSE-optimal beamforming in a narrowband single-user MISO system while taking into account imperfect CSI. Another work, [28], focuses on the design of an IRS-aided narrowband MU MISO system and considers the effect of imperfect CSI in their analysis. The authors in [29] propose a robust IRS design (with on/off reflection) for a narrowband single-user MISO system. They use the penalized Dinkelbach method to optimize the IRS reflection coefficients to maximize the achievable rate under CSI errors. In [30], the authors address a narrowband MU MISO scheme under imperfect CSI, considering only single-antenna users and the error model associated with the cascaded channels. In [21], the authors also consider a robust design of a narrowband MU MISO system based on a suboptimal solution to a rate maximization problem. In [31], the authors consider a narrowband MU (single-antenna) MISO IRS-aided system with on/off reflections at the IRS and focus on

maximizing the achievable rate under imperfect CSI. In [15], the authors investigate a MIMO CR system, where a secondary transmitter serves multiple secondary receivers concurrently. The design of the IRS matrix, precoding, and reception filters is considered under the presence of imperfect CSI at the secondary transmitter by using a norm-bounded error model. In [32], the authors address a narrowband vehicular MU IRS-aided communication system under imperfect CSI. They approach the joint precoder and IRS design by considering the outage probability constraint. Additionally, this work explores the concept of an active IRS, simplifying the design process under imperfect CSI by estimating the cascaded channel in two separate steps as in [28]: first, estimating the BS-IRS channel, and then estimating the IRS-user channels. However, this channel estimation strategy is impractical for passive IRSs. To highlight the novelty of the proposed scheme, a brief comparison with existing works in the literature is provided in Table I.

#### A. Contributions and organization

Unlike the aforementioned references [15, 18–25, 27–32], this work considers an IRS-aided wideband MU MIMO system with a passive IRS and imperfect CSI. We address the joint optimization of the frequency-dependent precoders/filters and the frequency-flat IRS phase-shift matrix, assuming imperfect CSI at the transmitter and receivers. We consider the intrinsic characteristics of IRS-aided systems, especially those with passive IRSs, to model imperfect CSI and develop a robust solution. In our approach, the estimation errors jointly affect both links in the cascaded channel, since we can only obtain an aggregated CSI from the IRS-involved channels, unlike the approaches in [28, 32].

We develop an alternating approach that minimizes the mean square error (MSE) between the original and estimated symbols by exploiting the BC-MAC duality. At each iteration, the updates are based on the BC-MAC duality and a projected gradient (PG) algorithm. We consider the specific characteristics of the MAC-BC and BC-MAC dualities when considering the deployment of an IRS and the conformation of the cascaded channel. The proposed alternating minimization algorithm iterates over the precoders/combiners in both the downlink and the uplink systems at each subcarrier, while also performing iterations over the frequency-flat IRS using a gradient descent step.

The proposed approach leads to better performance in terms of achievable sum-rate and MSE over baseline strategies. More specifically, the main contributions of this work are the following:

- We jointly design frequency-dependent precoders/filters and the frequency-flat IRS phase-shift matrix in a multistream wideband IRS-aided MU MIMO downlink by exploiting BC-MAC duality for aggregated imperfect CSI in passive IRS-aided systems. We also employ a PG algorithm to configure the IRS phase-shift matrix.
- We have developed an alternating minimization method to design the wideband precoders/filters and the frequency-flat IRS phase-shift matrix under imperfect CSI in the

TABLE I  
CONTRASTING THE CONTRIBUTIONS OF OUR SCHEME TO THE STATE-OF-THE-ART.

	Perfect CSI							Imperfect CSI								
	[18]	[19]	[20]	[22]	[23]	[24]	[25]	[15]	[21]	[27]	[28]	[29]	[30]	[31]	[32]	Our scheme
MIMO	×	✓	×	×	×	✓	×	✓	×	×	×	×	×	×	×	✓
Multuser	×	×	✓	✓	✓	✓	✓	×	✓	×	✓	×	✓	✓	✓	✓
Wideband	×	×	×	×	×	×	✓	×	×	×	×	×	×	×	×	✓
mmWave	×	×	×	×	×	×	×	×	✓	×	×	×	×	×	×	✓
Passive IRS	✓	✓	✓	✓	✓	✓	✓	×	✓	✓	✓	✓	✓	✓	×	✓

IRS-involved channels. The key aspect of this method is its consideration of the statistics of channel estimation errors to improve system performance. Moreover, this approach is independent of the specific statistics of the channel estimation errors.

The remainder of this work is organized as follows. The system model is described in Section II while the MMSE design is explained in Section III. An alternating minimization algorithm for the joint computation of the wideband BS precoders and user combiners, as well as the frequency-flat IRS-phase shift matrix, is described in Section IV by considering imperfect CSI. Convergence analysis for the proposed algorithm is carried out in Section V. Computational complexity analysis is exposed in Section VI. Simulation results are presented in Section VII and, finally, Section VIII is devoted to the conclusions.

### B. Notation

The following notation will be employed throughout the entire work:  $a$  is a scalar,  $\mathbf{a}$  is a vector, and  $\mathbf{A}$  is a matrix.  $[\mathbf{A}]_{i,j}$  is the entry on the  $i$ -th row and the  $j$ -th column of  $\mathbf{A}$ . Transpose and conjugate transpose of  $\mathbf{A}$  are represented by  $\mathbf{A}^T$  and  $\mathbf{A}^*$ , respectively.  $\|\mathbf{A}\|_F^2$  and  $\text{tr}[\mathbf{A}]$  denote the Frobenius norm and the trace of  $\mathbf{A}$ , respectively.  $\mathbf{A}^\dagger$  represents the pseudoinverse of  $\mathbf{A}$ . Calligraphic letters are employed to denote sets. The operator  $\text{blkdiag}(\cdot)$  constructs a block diagonal matrix from its input matrices. Finally, the expectation is denoted by  $\mathbb{E}[\cdot]$ ,  $\otimes$  is the column-wise Khatri-Rao product, and  $\otimes$  represents the Kronecker product.

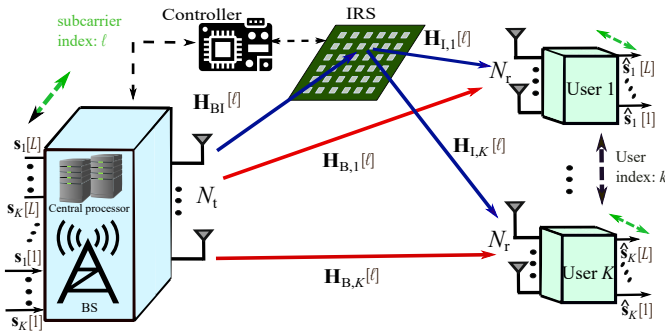


Fig. 1. Block diagram of the multistream wideband downlink MU IRS-aided mmWave MIMO system.

## II. SYSTEM MODEL

Let us consider the IRS-aided MU MIMO downlink shown in Fig. 1 where a common BS with  $N_t$  antennas communicates

with  $K$  users with  $N_r$  antennas each. The BS sends wideband OFDM symbols to fully exploit the large bandwidths available in mmWave. The wireless channels between the BS, the IRSs and the users are assumed to be frequency selective. The OFDM modulation is also assumed to have  $L$  subcarriers and a cyclic prefix long enough to avoid inter-symbol interference (ISI). This way, the frequency-selective channels are decomposed into  $L$  parallel narrowband subchannels, each experiencing a different frequency response.

We also consider multistream transmission in such a way that the BS allocates  $N_{s,k}[\ell]$  streams to be transmitted to the user  $k \in \{1, \dots, K\}$  at the subcarrier  $\ell \in \{1, \dots, L\}$ . The total number of streams allocated at subcarrier  $\ell$  is  $N_s[\ell] = \sum_{k=1}^K N_{s,k}[\ell]$  and the total number of streams considering all the subcarriers is  $N_s = \sum_{\ell=1}^L N_s[\ell]$ . At each channel use, the BS transmits to the  $k$ -th user at subcarrier  $\ell$  the vector of zero-mean symbols  $\mathbf{s}_k[\ell] = [s_{k1}[\ell], s_{k2}[\ell], \dots, s_{kN_{s,k}[\ell]}[\ell]]^T$  with  $\mathbb{E}[\mathbf{s}_k[\ell]\mathbf{s}_k^*[\ell]] = \mathbf{I}_{N_{s,k}[\ell]}$ . We assume there is no blockage between the BS and the users, i.e., a direct channel is available between the BS and the  $k$ -th user whose response at subcarrier  $\ell$  is  $\mathbf{H}_{B,k}[\ell] \in \mathbb{C}^{N_r \times N_t}$ .

In addition, the IRS introduces an additional cascaded BS-IRS-User link. The channel responses from the IRS to the  $k$ -th user and from the BS to the IRS at subcarrier  $\ell$  are represented by  $\mathbf{H}_{I,k}[\ell] \in \mathbb{C}^{N_r \times N}$  and  $\mathbf{H}_{BI}[\ell] \in \mathbb{C}^{N \times N_t}$ , respectively. The deployed IRS is assumed to have  $N$  passive elements and its phase-shift matrix is represented by the diagonal matrix  $\Theta = \text{diag}(\boldsymbol{\nu}) \in \mathcal{D}$ , where  $\boldsymbol{\nu} = [\nu_1, \dots, \nu_N]^T = [e^{j\theta_1}, \dots, e^{j\theta_N}]^T$  and  $\theta_n \in [0, 2\pi) \forall n$  is the phase shift introduced by the  $n$ -th IRS element.  $\mathcal{D} \in \mathbb{C}^{N \times N}$  is the set of feasible IRS matrices, i.e., the set of diagonal matrices with unit magnitude diagonal entries. The cascaded BS-IRS-user channel response at subcarrier  $\ell$  is given by  $\mathbf{H}_{c,k}[\ell] = \mathbf{H}_{I,k}[\ell]\Theta\mathbf{H}_{BI}[\ell] = \sum_{n=1}^N \nu_n \mathbf{h}_{I,k,n}[\ell]\mathbf{h}_{BI,n}^T[\ell]$ , where  $\mathbf{h}_{I,k,n}[\ell]$  and  $\mathbf{h}_{BI,n}[\ell]$  denote the  $n$ -th column of  $\mathbf{H}_{I,k}[\ell]$  and  $\mathbf{H}_{BI}[\ell]$ , respectively. We highlight that the frequency response of the IRS is nominally flat and, thus, common to all the subcarriers and users. As explained later, this circumstance makes the design of the IRS-aided communication system significantly more difficult.

The BS employs the linear precoder  $\mathbf{P}_k[\ell] \in \mathbb{C}^{N_t \times N_{s,k}[\ell]}$  to communicate with the  $k$ -th user at subcarrier  $\ell$ . As in [33, 34], these precoders are subject to the per-subcarrier transmission power constraint  $\sum_{k=1}^K \|\mathbf{P}_k[\ell]\|_F^2 \leq P_T[\ell]$  where  $P_T[\ell]$  is the available power at subcarrier  $\ell$ . For the sake of simplicity, and due to the optimality at high signal-to-noise ratios (SNRs), we will assume that  $P_T[\ell] = \frac{P_T}{L}$ , where  $P_T$  is the total power

available at transmission.<sup>1</sup> The signal received by the  $k$ -th user at subcarrier  $\ell$  is given by

$$\mathbf{y}_k[\ell] = \left( \underbrace{\mathbf{H}_{B,k}[\ell]}_{\text{Direct link}} + \underbrace{\mathbf{H}_{I,k}[\ell]\Theta\mathbf{H}_{BI}[\ell]}_{\text{IRS-aided link}} \right) \sum_{u=1}^K \mathbf{P}_u[\ell] \mathbf{s}_u[\ell] + \boldsymbol{\eta}_k[\ell], \quad (1)$$

where  $\boldsymbol{\eta}_k[\ell] = [\eta_{k1}, \eta_{k2}, \dots, \eta_{kN_r}]^T$  represents the complex-valued additive white Gaussian noise (AWGN) modeled as  $\boldsymbol{\eta}_k[\ell] \sim \mathcal{N}_{\mathbb{C}}(\mathbf{0}, \mathbf{C}_{\eta_k})$ . Finally, the equivalent channel response corresponding to the  $k$ -th user at subcarrier  $\ell$  is defined as

$$\begin{aligned} \mathbf{H}_{e,k}[\ell] &= \mathbf{H}_{B,k}[\ell] + \mathbf{H}_{I,k}[\ell]\Theta\mathbf{H}_{BI}[\ell] \\ &= \mathbf{H}_{B,k}[\ell] + \sum_{n=1}^N \nu_n \mathbf{h}_{I,k,n}[\ell] \mathbf{h}_{BI,n}^T[\ell], \end{aligned} \quad (2)$$

where  $n \in \{1, \dots, N\}$  stands for the index of each IRS element to modify each channel path by introducing the phase shift corresponding to the coefficient  $\nu_n = e^{j\theta_n}$ .

#### A. Channel estimation

To carry out the CSI estimation, pilot symbols without precoding are transmitted by the BS during  $N_p$  channel uses. The matrix  $\mathbf{X}[\ell] \in \mathbb{C}^{N_p \times N_t}$  comprises all the pilots transmitted at subcarrier  $\ell$ . Each row vector in  $\mathbf{X}[\ell]$  represents the pilots transmitted in the corresponding channel use.<sup>2</sup> As discussed in [36], we assume that  $N_p = N_t$  and  $\mathbf{X}[\ell]$  is a weighted unitary matrix such that  $\|\mathbf{X}[\ell]\|_{\text{F}}^2 = \frac{P_T}{L} N_p$ .

The pilot symbols received by user  $k$  at subcarrier  $\ell$  are collected in the matrix  $\mathbf{Y}'_k[\ell] \in \mathbb{C}^{N_r \times N_p}$  represented as

$$\mathbf{Y}'_k[\ell] = \left( \underbrace{\mathbf{H}_{B,k}[\ell]}_{\text{Direct link}} + \underbrace{\mathbf{H}_{I,k}[\ell]\Theta\mathbf{H}_{BI}[\ell]}_{\text{IRS-aided link}} \right) \mathbf{X}[\ell] + \mathbf{N}'_k[\ell]. \quad (3)$$

Columns of  $\mathbf{N}'_k[\ell]$  are mutually independent AWGN vectors distributed as  $\mathcal{N}_{\mathbb{C}}(\mathbf{0}, \mathbf{C}_{\eta_k})$ . By vectorizing  $\mathbf{Y}'_k[\ell]$  we get (cf. [37, Theorem 3.13])

$$\mathbf{y}'_k[\ell] = (\mathbf{X}[\ell] \otimes \mathbf{I}_{N_r}) \mathbf{h}_k[\ell] \boldsymbol{\nu}' + \boldsymbol{\eta}'_k[\ell], \quad (4)$$

where  $\boldsymbol{\nu}' = [1, \boldsymbol{\nu}^T]^T \in \mathbb{C}^{N+1}$ ,

$$\mathbf{h}_k[\ell] = [\mathbf{h}_{B,k}[\ell], \mathbf{H}_{BI}^T[\ell] \otimes \mathbf{H}_{I,k}[\ell]] \in \mathbb{C}^{N_r N_t \times N+1} \quad (5)$$

stacks both the vectorized versions of the direct channel  $\mathbf{h}_{B,k}[\ell] = \text{vec}(\mathbf{H}_{B,k}[\ell])$  and the cascaded channel, and  $\boldsymbol{\eta}'_k \sim \mathcal{N}_{\mathbb{C}}(\mathbf{0}, \mathbf{I}_{N_t} \otimes \mathbf{C}_{\eta_k})$ . Assuming  $N_\nu$  different phase allocations during the estimation process to modify the paths of the whole channel, we have

$$\mathbf{V} = [\boldsymbol{\nu}'_1, \dots, \boldsymbol{\nu}'_{N_\nu}] \in \mathbb{C}^{(N+1) \times N_\nu}. \quad (6)$$

As discussed in [36], we set  $N_\nu = N+1$  and  $\mathbf{V}$  is a weighted unitary matrix with unit-magnitude entries, e.g., a DFT or Hadamard matrix, such that  $\|\mathbf{V}\|_{\text{F}}^2 = (N+1)^2$ . We next assume that the same pilot matrix  $\mathbf{X}[\ell]$  is transmitted over

<sup>1</sup>We assume that all the computation related to the system design is performed at the BS, which serves as the resource allocator.

<sup>2</sup>The reduction of estimated overhead in MU schemes is beyond the scope of the paper. However, interested readers can refer to [35] for further exploration of this topic.

the  $N_\nu$  different phase allocations and that the corresponding received symbols are stacked in the following matrix

$$\mathbf{Y}_k[\ell] = (\mathbf{X}[\ell] \otimes \mathbf{I}) \mathbf{h}_k[\ell] \mathbf{V} + \mathbf{N}_k[\ell] \in \mathbb{C}^{N_r N_p \times N_\nu}. \quad (7)$$

Note now that the channel response  $\mathbf{h}_k[\ell]$  for the  $k$ -th user can be estimated following a least squares (LS) approach. Indeed, the LS estimation of the channel response is given by

$$\hat{\mathbf{H}}_{\text{LS},k}[\ell] = (\mathbf{X}[\ell] \otimes \mathbf{I})^\dagger \mathbf{Y}_k[\ell] \mathbf{V}^\dagger \in \mathbb{C}^{N_r N_t \times N+1}, \quad (8)$$

and the LS estimation error is given by the following matrix

$$\mathbf{N}_{\text{LS},k}[\ell] = (\mathbf{X}[\ell] \otimes \mathbf{I})^\dagger \mathbf{N}[\ell] \mathbf{V}^\dagger \in \mathbb{C}^{N_r N_t \times N+1}, \quad (9)$$

whose independent columns have the distribution  $\mathcal{N}_{\mathbb{C}}(\mathbf{0}, \mathbf{C}_{\text{LS},k})$  with the following covariance matrix

$$\mathbf{C}_{\text{LS},k} = \left( (\mathbf{X}^*[\ell] \mathbf{X}[\ell])^{-1} \otimes \mathbf{C}_{\eta_k} \right) \text{tr} \left( (\mathbf{V} \mathbf{V}^*)^{-1} \right) \in \mathbb{C}^{N_r N_t \times N_r N_t}, \quad (10)$$

where  $\mathbf{C}_{\eta_k} \in \mathbb{C}^{N_r \times N_r}$  is the receiving noise covariance matrix.

Leveraging the assumptions for  $\mathbf{X}[\ell]$  and  $\mathbf{V}$ , that is,  $\mathbf{X}^*[\ell] \mathbf{X}[\ell] = \frac{P_T}{L} \mathbf{I}_{N_t}$  and  $\mathbf{V} \mathbf{V}^* = (N+1) \mathbf{I}_{N+1}$ , leads to

$$\mathbf{C}_{\text{LS},k} = \left( \frac{L}{P_T} \mathbf{I}_{N_t} \otimes \mathbf{C}_{\eta_k} \right),$$

and every column of  $\mathbf{N}_{\text{LS},k}[\ell]$  has the distribution  $\mathcal{N}_{\mathbb{C}}(\mathbf{0}, \frac{L}{P_T} \mathbf{I}_{N_t} \otimes \mathbf{C}_{\eta_k})$ .

According to the above analysis, the channel uncertainty can be modeled as an statistical error. Therefore, channel realizations in the downlink can be decomposed as follows

$$\mathbf{H}_{B,k}[\ell] = \hat{\mathbf{H}}_{B,k}[\ell] + \mathbf{E}_{B,k}[\ell]$$

for the direct channels and

$$\mathbf{H}_{I,k}[\ell] \Theta \mathbf{H}_{BI}[\ell] = \sum_{n=1}^N \nu_n \left( \hat{\mathbf{H}}_{c,k,n}[\ell] + \mathbf{E}_{c,k,n}[\ell] \right),$$

for the cascaded channels such that

$$\hat{\mathbf{H}}_{c,k,n}[\ell] = \overline{\mathbf{h}_{I,k,n}[\ell] \mathbf{h}_{BI,n}^T[\ell]}, \forall n = 1, \dots, N. \quad (11)$$

Note that the estimate  $\overline{\mathbf{h}_{I,k,n}[\ell] \mathbf{h}_{BI,n}^T[\ell]}$  eventually is not rank-one due to the noise. Here,  $\mathbf{H}_{I,k}[\ell]$ ,  $\mathbf{H}_{BI}[\ell]$  and  $\mathbf{H}_{B,k}[\ell]$  are the true channels at subcarrier  $\ell$  of user  $k$  whereas  $\hat{\mathbf{H}}_{c,k}[\ell]$ , and  $\hat{\mathbf{H}}_{B,k}[\ell]$  stand for the estimated channels at subcarrier  $\ell$  of user  $k$ .

Recall that the estimations of the channels  $\mathbf{H}_{I,k}[\ell]$  and  $\mathbf{H}_{BI}[\ell]$  have to be performed jointly due to the passive nature of the IRS. The entries of  $\mathbf{E}_{B,k}[\ell]$  and  $\mathbf{E}_{c,k,n}[\ell]$  are the estimation errors of the direct and cascaded channels, respectively. These errors are zero-mean Gaussian distributed with a covariance matrix  $\mathbb{E}[\mathbf{e}_{B,k}[\ell] \mathbf{e}_{B,k}^*[\ell]] = \mathbf{C}_{\text{LS},k}, \forall \ell$  and  $\mathbb{E}[\mathbf{e}_{c,k,n}[\ell] \mathbf{e}_{c,k,n}^*[\ell]] = \mathbf{C}_{\text{LS},k}, \forall \ell, n$ , respectively, where  $\mathbf{e}_{B,k}[\ell]$  and  $\mathbf{e}_{c,k,n}[\ell]$  are the vectorized versions of  $\mathbf{E}_{B,k}[\ell], \forall k, \ell$  and  $\mathbf{E}_{c,k,n}[\ell], \forall k, n, \ell$ , respectively. They correspond to the first and the  $(n+1)$ -th column of  $\mathbf{N}_{\text{LS},k}[\ell]$ , respectively. Therefore, note that the mutually independent columns of  $\mathbf{E}_{B,k}[\ell]$  and  $\mathbf{E}_{c,k,n}[\ell]$  are distributed as  $\mathcal{N}_{\mathbb{C}}(\mathbf{0}, \frac{L}{P_T} \mathbf{C}_{\eta_k})$ . According to this error model, the next equivalence can be stated

$$\mathbf{H}_{e,k}[\ell] = \hat{\mathbf{H}}_{e,k}[\ell] + \mathbf{E}_{B,k}[\ell] + \sum_{n=1}^N \nu_n \mathbf{E}_{c,k,n}[\ell], \quad (12)$$

where

$$\hat{\mathbf{H}}_{e,k}[\ell] = \hat{\mathbf{H}}_{B,k}[\ell] + \sum_{n=1}^N \nu_n \hat{\mathbf{H}}_{e,k,n}[\ell]. \quad (13)$$

Note that considering the channel estimation errors, the received symbols given by (1) can be expressed as follows

$$\begin{aligned} \mathbf{y}_k[\ell] &= \left( \hat{\mathbf{H}}_{e,k}[\ell] + \mathbf{E}_{B,k}[\ell] + \sum_{n=1}^N \nu_n \mathbf{E}_{e,k,n}[\ell] \right) \\ &\quad \times \sum_{u=1}^K \mathbf{P}_u[\ell] \mathbf{s}_u[\ell] + \boldsymbol{\eta}_k[\ell]. \end{aligned} \quad (14)$$

At reception, the user  $k$  estimates its symbols  $\hat{\mathbf{s}}_k[\ell]$  at subcarrier  $\ell$  by applying the linear filter  $\mathbf{W}_k[\ell] \in \mathbb{C}^{N_{s,k}[\ell] \times N_r}$ , that is,  $\hat{\mathbf{s}}_k[\ell] = \mathbf{W}_k[\ell] \mathbf{y}_k[\ell]$  (see Fig. 2).

The previous imperfect CSI model has been developed from a transmitting perspective. However, the same CSI model will be considered when designing the receiving filters. Although this is a simplifying assumption, it is a conservative one since we can expect that the CSI estimation quality at the receivers will be better than that at the transmitter. Considering imperfect CSI at the receivers requires the implementation of compensation techniques, similar to those described in [38], to enable coherent detection at the receivers. We assumed that the estimations of the channels (the direct channels and the cascaded channels) are sent back from the users to the BS through the feedback channel. In practical scenarios, systems with limited rate CSI feedback suffers from erroneous CSI at the transmitter, which is why we assume imperfect CSI at both sides. The delay effect of the feedback channel is disregarded because is relatively easy to correct ([39]) but at the expense of needlessly complicating our notation.

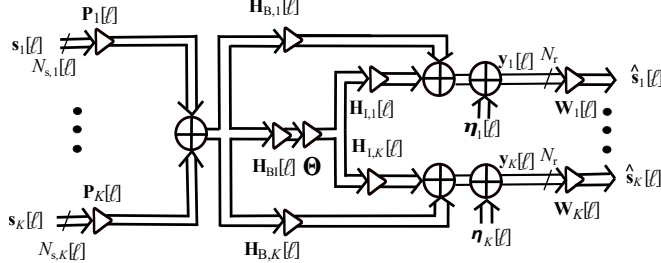


Fig. 2. Multistream wideband downlink MU IRS-aided mmWave MIMO system at subcarrier  $\ell$ .

Table II summarizes the main system model parameters and variables considered in this multistream wideband downlink MU IRS-aided mmWave MIMO system under imperfect CSI.

### B. Channel model

The channels for the different mmWave system links are assumed to be time-dispersive. The channel response matrices at the  $m$ -th delay tap with  $m \in \{0, \dots, L_D - 1\}$ , where  $L_D$  is the maximum number of delay taps, are considered as follows [34, 40, 41]

$$\mathbf{H}_{\text{temp}}[m] = \gamma \sum_{j=1}^{N_{\text{path}}} \beta_j p_{rc}(mT_s - \tau_j) \mathbf{a}_r(\phi_j^t, \psi_j^r) \mathbf{a}_t^*(\phi_j^t, \psi_j^t), \quad (15)$$

TABLE II  
DOWNLINK SYSTEM MODEL PARAMETERS.

Parameter	Setting
Number of antennas at the BS	$N_t$
Number of users	$K$
Number of antennas per users	$N_r$
Number of subcarriers	$L$
Number of streams per user at subcarrier $\ell$	$N_{s,k}[\ell]$
Vector of the $N_{s,k}[\ell]$ symbols at subcarrier $\ell$	$\mathbf{s}_k[\ell]$
$k$ -th BS precoder at subcarrier $\ell$	$\mathbf{P}_k[\ell]$
Power available at subcarrier $\ell$	$P_T[\ell]$
BS-User direct channel at subcarrier $\ell$	$\mathbf{H}_{B,k}[\ell]$
BS-IRS channel subcarrier $\ell$	$\mathbf{H}_{B1}[\ell]$
IRS-User channel at subcarrier $\ell$	$\mathbf{H}_{I,k}[\ell]$
Frequency-flat IRS phase shift matrix	$\Theta$
Main diagonal of IRS phase shift matrix	$\nu$
Vector of AWGN at the $k$ -th user at subcarrier $\ell$	$\boldsymbol{\eta}_k[\ell]$
$k$ -th user filter at subcarrier $\ell$	$\mathbf{W}_k[\ell]$
$N_{s,k}[\ell]$ estimated symbols at subcarrier $\ell$	$\hat{\mathbf{s}}_k[\ell]$
Total number of streams at subcarrier $\ell$	$N_s[\ell]$
Total number of data streams	$N_s$
Covariance matrices of the errors in the downlink	$\mathbf{C}\boldsymbol{\eta}_k$

where  $N_{\text{path}}$  is the number of channel paths,  $p_{rc}(t)$  represents the raised cosine pulse-shaping filter,  $\tau_j$  is the relative delay for the  $j$ -th path,  $T_s$  is the sampling period,  $\gamma = \sqrt{N_t N_r / N_{\text{path}}}$  is a power normalization factor and  $\beta_j$  stands for the complex path gain for the  $j$ -th channel path. The term  $\phi^t(\psi^t)$  stands for the azimuth (elevation) angles of departure (AoD) and  $\phi^r(\psi^r)$  are the azimuth (elevation) angles of arrival (AoA). In the frequency domain, the channel response (15) can be represented as [9]

$$\begin{aligned} \mathbf{H}[\ell] &= \sum_{m=0}^{L_D-1} \mathbf{H}_{\text{temp}}[m] e^{j2\pi m(\ell-1)/L} \\ &= \sum_{j=1}^{N_{\text{path}}} \beta_j[\ell] \mathbf{a}_r[\ell](\phi_j^r, \psi_j^r) \mathbf{a}_t^*[\ell](\phi_j^t, \psi_j^t), \end{aligned} \quad (16)$$

where  $\ell \in \{1, \dots, L\}$  and  $\beta_j[\ell]$  represents the  $j$ -th path gain at subcarrier  $\ell$  and corresponds to

$$\beta_j[\ell] = \gamma \beta_j \sum_{m=0}^{L_D-1} p_{rc}(mT_s - \tau_n) e^{j2\pi m(\ell-1)/L}.$$

We assume uniform planar arrays (UPAs) with dimensions  $N_a \times N_b$  at both communication ends. Therefore, the array response vectors  $\mathbf{a}_t(\phi^t, \psi^t)$  and  $\mathbf{a}_r(\phi^r, \psi^r)$  have the form [42]

$$\begin{aligned} \mathbf{a}(\phi, \psi) &= \frac{1}{\sqrt{N_a N_b}} \left[ 1, e^{j \frac{2\pi}{f_\ell} c d (\sin \phi \sin \psi + \cos \psi)}, \dots, \right. \\ &\quad \left. e^{j \frac{2\pi}{f_\ell} c d ((N_a-1) \sin \phi \sin \psi + (N_b-1) \cos \psi)} \right]^T \end{aligned}$$

where  $f_\ell$  is the frequency corresponding to the  $\ell$ -th subcarrier,  $c$  is the speed of light, and  $d$  is the inter antenna spacing which is often set to  $\lambda/2$ , with  $\lambda = \frac{c}{f_c}$  the wavelength corresponding to the carrier frequency  $f_c$ .

### C. Achievable sum-rate

Considering the described scenario (see also Fig. 2) and imperfect CSI model, we aim at determining the precoders

$\mathbf{P}_k[\ell], \forall k, \ell$ , the receiving linear filters  $\mathbf{W}_k[\ell], \forall k, \ell$ , and the IRS phase shift matrix  $\Theta$  which maximize the achievable sum-rate given by<sup>3</sup>

$$R_{\text{sum}} = \sum_{\ell=1}^L \sum_{k=1}^K \log_2 \det \left( \mathbf{I}_{N_{s,k}[\ell]} + \mathbf{X}_k^{-1}[\ell] \mathbf{W}_k[\ell] \mathbf{H}_{e,k}[\ell] \mathbf{P}_k[\ell] \mathbf{P}_k^*[\ell] \mathbf{H}_{e,k}^*[\ell] \mathbf{W}_k^*[\ell] \right) \quad (17)$$

with

$$\mathbf{X}_k[\ell] = \sum_{i \neq k} \mathbf{W}_k[\ell] \mathbf{H}_{e,k}[\ell] \mathbf{P}_i[\ell] \mathbf{P}_i^*[\ell] \mathbf{H}_{e,k}^*[\ell] \mathbf{W}_k^*[\ell] + \mathbf{W}_k[\ell] \mathbf{C}_{\eta_k} \mathbf{W}_k^*[\ell], \quad (18)$$

while fulfilling the overall power constraint ( $P_T$ ). Recall that  $\mathbf{H}_{e,k}[\ell]$  represents the equivalent BS-IRS-User channel for user  $k$  at subcarrier  $\ell$ . Accordingly, we formulate the following optimization problem<sup>4</sup>

$$\begin{aligned} & \arg \max_{\Theta, \mathbf{P}_k[\ell], \mathbf{W}_k[\ell], \forall k, \ell} R_{\text{sum}} \\ & \text{s.t. } \sum_{k=1}^K \text{tr}(\mathbf{P}_k[\ell] \mathbf{P}_k^*[\ell]) \leq P_T[\ell], \forall \ell, \Theta \in \mathcal{D}. \end{aligned} \quad (19)$$

The solution to (19) is computationally intractable mainly because of the coupling of the variables  $\mathbf{P}_k$  and  $\Theta$ , the non-convex nature of the cost function and the non-convex constraints on the IRS matrix, i.e., unit magnitude for each diagonal entry.

Furthermore, the IRS phase shift matrix is common to all the users and subcarriers which makes the solution of (19) even more difficult since the common IRS must be designed to simultaneously modify all the paths of the user channels at the  $L$  subcarriers. Note that the exhaustive search technique is required to find an optimal solution, but its impracticality arises due to the high computational complexity, even for moderate-sized systems. As a result, achieving a globally optimal solution for these complex wideband MU MIMO IRS-aided systems is not feasible.

### III. MMSE APPROACH

We reformulate the optimization problem (19) as an MSE minimization problem since minimizing the sum-MSE maximizes a lower bound of the system capacity [45]. Weighted MMSE could be used instead of sum MSE minimization, but this would require an additional inner iterative loop in our design algorithm to optimize the MSE weights [45]. Some performance improvement is to be expected but at the expense of a significant increase in computational complexity and a slowdown in convergence.

<sup>3</sup>While robust design and statistical approaches under imperfect CSI in the transmitter often involve considering channel outages, our specific focus is on rate maximization, as exemplified in works such as [28] and [43].

<sup>4</sup>Note that a similar optimization problem could be formulated by considering an individual minimum data rate per user. This would entail changes in the kind of MAC-BC and BC-MAC dualities (second or third kind dualities [44]) explained below.

Let us elaborate the system model under imperfect CSI for the  $k$ -th user symbols at the  $\ell$ -th subcarrier after the linear filtering at reception, i.e.,

$$\begin{aligned} \hat{\mathbf{s}}_k[\ell] &= \mathbf{W}_k[\ell] \left( \hat{\mathbf{H}}_{e,k}[\ell] + \mathbf{E}_{B,k}[\ell] + \sum_{n=1}^N \nu_n \mathbf{E}_{c,k,n}[\ell] \right) \\ &\times \sum_{u=1}^K \mathbf{P}_u[\ell] \mathbf{s}_u[\ell] + \mathbf{W}_k[\ell] \boldsymbol{\eta}_k[\ell]. \end{aligned} \quad (20)$$

Thus, the downlink MSE for the  $k$ -th user at subcarrier  $\ell$  is

$$\begin{aligned} \text{MSE}_k^{\text{DL}}[\ell] &= \mathbb{E} [\|\mathbf{s}_k[\ell] - \hat{\mathbf{s}}_k[\ell]\|_2^2] \\ &= \text{tr} \left( \mathbf{W}_k[\ell] \left\{ \hat{\mathbf{H}}_{e,k}[\ell] \left[ \sum_{i=1}^K \mathbf{P}_i[\ell] \mathbf{P}_i^*[\ell] \right] \right. \right. \\ &\quad \times \left. \left. \hat{\mathbf{H}}_{e,k}^*[\ell] + \mathbf{C}_{\eta_k} \right\} \mathbf{W}_k^*[\ell] \right) \\ &+ \mathbb{E} \left[ \mathbf{W}_k[\ell] \left\{ \mathbf{E}_{B,k}[\ell] \left[ \sum_{i=1}^K \mathbf{P}_i[\ell] \mathbf{P}_i^*[\ell] \right] \mathbf{E}_{B,k}^*[\ell] \right\} \mathbf{W}_k^*[\ell] \right] \\ &+ \mathbb{E} \left[ \mathbf{W}_k[\ell] \left\{ \sum_{n=1}^N \mathbf{E}_{c,k,n}[\ell] \nu_n \left[ \sum_{i=1}^K \mathbf{P}_i[\ell] \mathbf{P}_i^*[\ell] \right] \right. \right. \\ &\quad \times \left. \left. \sum_{n'=1}^N \mathbf{E}_{c,k,n'}^*[\ell] \nu_{n'}^* \right\} \mathbf{W}_k^*[\ell] \right] \\ &- \mathbf{W}_k[\ell] \hat{\mathbf{H}}_{e,k}[\ell] \mathbf{P}_k[\ell] - \mathbf{P}_k^*[\ell] \hat{\mathbf{H}}_{e,k}^*[\ell] \mathbf{W}_k^*[\ell] + \mathbf{I}_{N_{s,k}[\ell]} \Big). \end{aligned} \quad (21)$$

This expression for the downlink MSE in terms of the precoders  $\mathbf{P}_k[\ell]$ , the filters  $\mathbf{W}_k[\ell]$ , the estimated channels  $\hat{\mathbf{H}}_{e,k}[\ell]$  and the errors  $\mathbf{E}_{B,k}[\ell]$ ,  $\mathbf{E}_{c,k,n}[\ell], \forall n, k$  can be rewritten as follows

$$\begin{aligned} \text{MSE}_k^{\text{DL}}[\ell] &= \text{tr} \left( \mathbf{W}_k[\ell] \left\{ \hat{\mathbf{H}}_{e,k}[\ell] \left[ \sum_{i=1}^K \mathbf{P}_i[\ell] \mathbf{P}_i^*[\ell] \right] \right. \right. \\ &\quad \times \left. \left. \hat{\mathbf{H}}_{e,k}^*[\ell] + \mathbf{C}_{\eta_k} \right\} \mathbf{W}_k^*[\ell] \right) \\ &+ \text{tr} \left( \sum_{i=1}^K \mathbf{P}_i[\ell] \mathbf{P}_i^*[\ell] \right) \text{tr} \left( \mathbf{W}_k[\ell] \mathbf{C}_{\eta_k} \mathbf{W}_k^*[\ell] \right) \frac{L}{P_T} \\ &+ \nu^* \text{tr} \left( \sum_{i=1}^K \mathbf{P}_i[\ell] \mathbf{P}_i^*[\ell] \right) \text{tr} \left( \mathbf{W}_k[\ell] \mathbf{C}_{\eta_k} \mathbf{W}_k^*[\ell] \right) \nu \frac{L}{P_T} \\ &- \text{tr} \left( \mathbf{W}_k[\ell] \hat{\mathbf{H}}_{e,k}[\ell] \mathbf{P}_k[\ell] - \mathbf{P}_k^*[\ell] \hat{\mathbf{H}}_{e,k}^*[\ell] \mathbf{W}_k^*[\ell] + \mathbf{I}_{N_{s,k}[\ell]} \right), \end{aligned} \quad (22)$$

where the independence of the columns of  $\mathbf{E}_{B,k}[\ell]$  and  $\mathbf{E}_{c,n,k}[\ell]$  has been exploited. Note that (22) contains the covariance matrices  $\frac{L}{P_T} \mathbf{C}_{\eta_k}$  of the error matrices  $\mathbf{E}_{B,k}[\ell]$  and  $\mathbf{E}_{c,n,k}[\ell]$ . Hence, the statistical information of the channel estimation errors is incorporated in (22). Although we assumed the LS method for channel estimation in Section II-A, our proposed solution is not limited to this error model in passive IRS-aided systems. Equation (22) is independent of

the specific error models used for aggregated CSI estimation in (11) and can be adapted to various channel estimation techniques with different covariance matrices for the errors.

For given precoders  $\mathbf{P}_k[\ell]$  and IRS phase shift matrix  $\Theta$ , the  $k$ -th user's MMSE receiving filter is readily determined as

$$\mathbf{W}_{\text{MMSE},k}[\ell] = \mathbf{P}_k^*[\ell] \hat{\mathbf{H}}_{e,k}^*[\ell] \left( \hat{\mathbf{H}}_{e,k}[\ell] \mathbf{P}_k[\ell] \mathbf{P}_k^*[\ell] \hat{\mathbf{H}}_{e,k}^*[\ell] + \mathbf{C}_{\text{IN},k}[\ell] \right)^{-1} \quad (23)$$

where  $\mathbf{C}_{\text{IN},k}[\ell] \in \mathbb{C}^{N_r \times N_r}$  is the  $k$ -th interference-plus-noise covariance matrix given by

$$\begin{aligned} \mathbf{C}_{\text{IN},k}[\ell] &= \sum_{i \neq k} \hat{\mathbf{H}}_{e,i}[\ell] \mathbf{P}_i[\ell] \mathbf{P}_i^*[\ell] \hat{\mathbf{H}}_{e,i}^*[\ell] + \mathbf{C}_{\eta_k} \\ &+ (N+1) \sum_{i=1}^K \text{tr}(\mathbf{P}_i[\ell] \mathbf{P}_i^*[\ell]) \mathbf{C}_{\eta_k} \frac{L}{P_T}. \end{aligned} \quad (24)$$

Substituting (23) into (20) leads to the following expression for the downlink MSE

$$\text{MSE}_k^{\text{DL}}[\ell] = \text{tr}(\mathbf{I}_{N_s,k}[\ell] + \mathbf{P}_k^*[\ell] \hat{\mathbf{H}}_{e,k}^*[\ell] \mathbf{C}_{\text{IN},k}^{-1}[\ell] \hat{\mathbf{H}}_{e,k}[\ell] \mathbf{P}_k[\ell])^{-1}. \quad (25)$$

Finally, in order to determine the wideband precoders  $\mathbf{P}_k[\ell]$  and the IRS phase-shift matrix  $\Theta$  assuming imperfect CSI, we formulate the following downlink MSE minimization problem

$$\begin{aligned} \arg \min_{\Theta, \mathbf{P}_k[\ell], \forall k, \ell} & \sum_{\ell=1}^L \sum_{k=1}^K \text{MSE}_k^{\text{DL}}[\ell] \\ \text{s.t.} & \sum_{k=1}^K \text{tr}(\mathbf{P}_k[\ell] \mathbf{P}_k^*[\ell]) \leq P_T[\ell], \forall \ell, \Theta \in \mathcal{D}, \end{aligned} \quad (26)$$

with  $\text{MSE}_k^{\text{DL}}[\ell]$  given by (25) and considering  $\mathbf{C}_{\text{IN},k}[\ell]$  as in (24). In the ensuing section, this minimization problem will be formulated in the dual MAC in order to obtain a more appropriate mathematical structure for the MSE. This will lead to a significant reduction in computational complexity.

#### IV. PROPOSED SOLUTION

In this section, we will exploit the BC-MAC duality [44, 46] to solve (26). We start by defining the virtual dual MAC model for the considered scenario. Let  $\mathbf{s}_k^{\text{UL}}[\ell]$  with  $\mathbb{E}[\mathbf{s}_k^{\text{UL}}[\ell] \mathbf{s}_k^{\text{UL}*}[\ell]] = \mathbf{I}_{N_s,k}[\ell]$  be the zero-mean vector of uplink symbols transmitted by the users over subcarrier  $\ell$  in the dual MAC. The corresponding uplink symbols received at the BS will be (see Fig. 3)

$$\mathbf{y}^{\text{UL}}[\ell] = \sum_{k=1}^K \mathbf{H}_{e,k}^*[\ell] \mathbf{C}_{\eta_k}^{-1/2,*} \mathbf{T}_k[\ell] \mathbf{s}_k^{\text{UL}}[\ell] + \mathbf{n}[\ell], \quad (27)$$

where  $\mathbf{T}_k[\ell] \in \mathbb{C}^{N_r \times N_s,k}[\ell]$  and  $\mathbf{H}_{e,k}^*[\ell] \mathbf{C}_{\eta_k}^{-1/2,*}$  are the  $k$ -th user precoder and the equivalent channel response in the dual MAC, respectively, for subcarrier  $\ell$ . The noise at subcarrier  $\ell$  introduced at reception is represented by  $\mathbf{n}[\ell] \sim \mathcal{N}_{\mathcal{C}}(0, \mathbf{I}_{N_t})$ . Note that

$$\mathbf{H}_{e,k}^*[\ell] = \mathbf{H}_{\text{BI}}^*[\ell] \Theta^* \mathbf{H}_{\text{I},k}^*[\ell] + \mathbf{H}_{\text{B},k}^*[\ell] \quad (28)$$

is the conjugate transpose of the joint cascaded and direct channel matrices for the  $k$ -th user at subcarrier  $\ell$  given by

(2). We now introduce  $\mathbf{G}_k[\ell] \in \mathbb{C}^{N_s,k}[\ell] \times N_t$ ,  $\forall k$  which are the linear filters used at reception in the dual MAC to estimate the incoming uplink symbols for user  $k$  and subcarrier  $\ell$ , i.e.,

$$\begin{aligned} \hat{\mathbf{s}}_k^{\text{UL}}[\ell] &= \mathbf{G}_k[\ell] \mathbf{y}^{\text{UL}}[\ell] \\ &= \mathbf{G}_k[\ell] \sum_{i=1}^K \mathbf{H}_{e,i}^*[\ell] \mathbf{C}_{\eta_k}^{-1/2,*} \mathbf{T}_i[\ell] \mathbf{s}_i^{\text{UL}}[\ell] + \mathbf{G}_k[\ell] \mathbf{n}[\ell]. \end{aligned} \quad (29)$$

By considering imperfect CSI and a similar approach to that in Section II-A, the uplink symbol expression (29) can be rewritten as [cf. (12)]

$$\begin{aligned} \hat{\mathbf{s}}_k^{\text{UL}}[\ell] &= \mathbf{G}_k[\ell] \sum_{i=1}^K \left( \hat{\mathbf{H}}_{e,i}^*[\ell] + \mathbf{E}_{\text{B},i}^*[\ell] + \sum_{n=1}^N \mathbf{E}_{e,k,n}^*[\ell] \nu_n^* \right) \\ &\times \mathbf{C}_{\eta_k}^{-1/2,*} \mathbf{T}_i[\ell] \mathbf{s}_i^{\text{UL}}[\ell] + \mathbf{G}_k[\ell] \mathbf{n}[\ell]. \end{aligned} \quad (30)$$

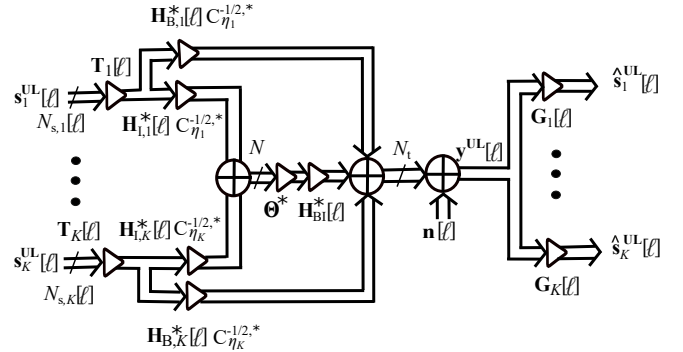


Fig. 3. Multistream wideband dual uplink MU IRS-aided mmWave MIMO system model at subcarrier  $\ell$ .

We next determine the uplink MSE between the sent and the estimated symbols, i.e.,  $\text{MSE}_k^{\text{UL}}[\ell] = \mathbb{E}[\|\mathbf{s}_k^{\text{UL}}[\ell] - \hat{\mathbf{s}}_k^{\text{UL}}[\ell]\|_2^2]$ . This MSE per user in the dual uplink at subcarrier  $\ell$ , when considering imperfect CSI, is given by

$$\begin{aligned} \text{MSE}_k^{\text{UL}}[\ell] &= \text{tr} \left( \mathbf{G}_k[\ell] \left\{ \left[ \sum_{i=1}^K \hat{\mathbf{H}}_{e,i}^*[\ell] \mathbf{C}_{\eta_k}^{-1/2,*} \mathbf{T}_i[\ell] \right. \right. \right. \\ &\times \left. \left. \left. \mathbf{T}_i^*[\ell] \mathbf{C}_{\eta_k}^{-1/2} \hat{\mathbf{H}}_{e,i}[\ell] \right] + \mathbf{I}_{N_t} \right\} \mathbf{G}_k^*[\ell] \right) \\ &+ \sum_{i=1}^K \text{tr} \left( \frac{L}{P_T} \mathbf{T}_i[\ell] \mathbf{T}_i^*[\ell] \right) \text{tr} \left( \mathbf{G}_k[\ell] \mathbf{G}_k^*[\ell] \right) (N+1) \\ &- \text{tr} \left( \mathbf{G}_k[\ell] \hat{\mathbf{H}}_{e,k}^*[\ell] \mathbf{C}_{\eta_k}^{-1/2,*} \mathbf{T}_k[\ell] \right. \\ &\left. - \mathbf{T}_k^*[\ell] \mathbf{C}_{\eta_k}^{-1/2} \hat{\mathbf{H}}_{e,k}[\ell] \mathbf{G}_k^*[\ell] + \mathbf{I}_{N_s,k}[\ell] \right), \end{aligned} \quad (31)$$

since  $\nu^* \nu = N$ . The MMSE filter in the uplink is given by

$$\begin{aligned} \mathbf{G}_{\text{MMSE},k}[\ell] &= \mathbf{T}_k^*[\ell] \mathbf{C}_{\eta_k}^{-1/2} \hat{\mathbf{H}}_{e,k}[\ell] \\ &\times \left( \hat{\mathbf{H}}_e^*[\ell] \mathbf{C}_{\eta_k}^{-1/2,*} \mathbf{T}[\ell] \mathbf{T}^*[\ell] \mathbf{C}_{\eta_k}^{-1/2} \hat{\mathbf{H}}_e[\ell] + \mathbf{I}_{N_t} \right. \\ &\left. + (1+N) \sum_{i=1}^K \text{tr} \left( \frac{L}{P_T} \mathbf{T}_i[\ell] \mathbf{T}_i^*[\ell] \right) \mathbf{I}_{N_t} \right)^{-1}, \end{aligned} \quad (32)$$



where  $\mathbf{T}[\ell] = \text{blkdiag}(\mathbf{T}_1[\ell], \dots, \mathbf{T}_K[\ell])$  is a block diagonal matrix that comprises all the dual uplink user precoders,  $\mathbf{C} = \text{blkdiag}(\mathbf{C}_{\eta_1}, \dots, \mathbf{C}_{\eta_K}) \in \mathbb{C}^{N_r K \times N_r K}$  is another block diagonal matrix stacking the inverse noise covariance matrices corresponding to all the users, and  $\hat{\mathbf{H}}_e^*[\ell] = [\hat{\mathbf{H}}_{e,1}^*[\ell], \dots, \hat{\mathbf{H}}_{e,K}^*[\ell]]$  stacks all the equivalent channel response matrices. The MSE per user achieved at subcarrier  $\ell$  when employing this MMSE receiving filter is

$$\begin{aligned} \text{MSE}_k^{\text{UL}}[\ell] = & \text{tr} \left[ \left( \mathbf{I}_{N_s, k}[\ell] + \mathbf{T}_k^*[\ell] \mathbf{C}_{\eta_k}^{-1/2} \hat{\mathbf{H}}_{e, k}[\ell] \right. \right. \\ & \times \left( \sum_{i \neq k}^K \hat{\mathbf{H}}_{e, i}^*[\ell] \mathbf{C}_{\eta_i}^{-1/2, *} \mathbf{T}_i[\ell] \mathbf{T}_i^*[\ell] \mathbf{C}_{\eta_i}^{-1/2} \hat{\mathbf{H}}_{e, i}[\ell] \right. \\ & \left. \left. + \mathbf{I}_{N_t} + (1+N) \sum_{i=1}^K \text{tr} \left( \frac{L}{P_T} \mathbf{T}_i[\ell] \mathbf{T}_i^*[\ell] \right) \mathbf{I}_{N_t} \right)^{-1} \right. \\ & \left. \times \hat{\mathbf{H}}_{e, k}^*[\ell] \mathbf{C}_{\eta_k}^{-1/2, *} \mathbf{T}_k[\ell] \right)^{-1} \Big], \quad (33) \end{aligned}$$

Note that this expression only depends on the uplink precoders in the dual MAC  $\mathbf{T}_k[\ell]$  and the IRS phase-shift matrix  $\Theta$ .

We next rewrite the received uplink symbols at subcarrier  $\ell$  given by (27) by means of the following more compact expression (cf. the definitions below (32))

$$\mathbf{y}^{\text{UL}}[\ell] = \mathbf{H}_e^*[\ell] \mathbf{C}_{\eta}^{-1/2, *} \mathbf{T}[\ell] \mathbf{s}^{\text{UL}}[\ell] + \mathbf{n}[\ell], \quad (34)$$

where  $\mathbf{s}^{\text{UL}}[\ell] = [\mathbf{s}_1^{\text{UL}, \text{T}}[\ell], \dots, \mathbf{s}_K^{\text{UL}, \text{T}}[\ell]]^{\text{T}}$  is a vector that gathers all the uplink user symbols sent over the  $\ell$ -th subcarrier. According to (2), this latter matrix is related to the different channel responses in the signal model as follows

$$\mathbf{H}_e^*[\ell] = (\mathbf{H}_{\text{BI}}^*[\ell] \Theta^* \mathbf{H}_{\text{I}}^*[\ell] + \mathbf{H}_{\text{B}}^*[\ell]) \in \mathbb{C}^{N_t \times N_r K}, \quad (35)$$

where  $\mathbf{H}_{\text{I}}^*[\ell] = [\mathbf{H}_{\text{I}, 1}^*[\ell], \dots, \mathbf{H}_{\text{I}, K}^*[\ell]] \in \mathbb{C}_{\eta}^{-1/2, *}$ , and  $\mathbf{H}_{\text{B}}^*[\ell] = [\mathbf{H}_{\text{B}, 1}^*[\ell], \dots, \mathbf{H}_{\text{B}, K}^*[\ell]] \in \mathbb{C}^{N_t \times N_r K}$ .

Substituting the frequency selective equivalent channel responses given by (35) into (34) leads to

$$\mathbf{y}^{\text{UL}}[\ell] = (\mathbf{H}_{\text{BI}}^*[\ell] \Theta^* \mathbf{H}_{\text{I}}^*[\ell] + \mathbf{H}_{\text{B}}^*[\ell]) \mathbf{C}_{\eta}^{-1/2, *} \mathbf{T}[\ell] \mathbf{s}^{\text{UL}}[\ell] + \mathbf{n}[\ell]. \quad (36)$$

Note that  $\mathbf{T}[\ell] \in \mathbb{C}^{N_r K \times N_s[\ell]}$  and  $\mathbf{s}^{\text{UL}}[\ell] \in \mathbb{C}^{N_s[\ell]}$  with  $N_s[\ell] = \sum_{k=1}^K N_{s, k}[\ell]$ , i.e., the dimensions of  $\mathbf{T}[\ell]$  and  $\mathbf{s}^{\text{UL}}[\ell]$  depend on the number of served data streams per user.

The estimated uplink data symbols corresponding to the  $K$  users at subcarrier  $\ell$  according to the dual MAC signal model can hence be defined as

$$\begin{aligned} \hat{\mathbf{s}}^{\text{UL}}[\ell] = & \mathbf{G}[\ell] (\mathbf{H}_{\text{BI}}^*[\ell] \Theta^* \mathbf{H}_{\text{I}}^*[\ell] + \mathbf{H}_{\text{B}}^*[\ell]) \\ & \times \mathbf{C}_{\eta}^{-1/2, *} \mathbf{T}[\ell] \mathbf{s}^{\text{UL}}[\ell] + \mathbf{G}[\ell] \mathbf{n}[\ell], \quad (37) \end{aligned}$$

where  $\mathbf{G}[\ell] = [\mathbf{G}_1^*[\ell], \dots, \mathbf{G}_K^*[\ell]]^*$  is the overall receive filter that comprises the filters  $\mathbf{G}_k^*[\ell]$ ,  $\forall k$  which estimate all the uplink symbols at subcarrier  $\ell$ . Note that  $\hat{\mathbf{s}}^{\text{UL}}[\ell]$  collects all the estimated user symbols  $\hat{s}_k^{\text{UL}}[\ell]$ ,  $\forall k$ , which can also be obtained through (29). Considering that the CSI is imperfect,

the estimated uplink user symbols  $\hat{\mathbf{s}}^{\text{UL}}[\ell]$  can be represented as follows

$$\begin{aligned} \hat{\mathbf{s}}^{\text{UL}}[\ell] = & \mathbf{G}[\ell] \left( \hat{\mathbf{H}}_{\text{B}}^*[\ell] + \mathbf{E}_{\text{B}}^*[\ell] + \sum_{n=1}^N (\hat{\mathbf{H}}_{e, n}^*[\ell] + \mathbf{E}_{e, n}^*[\ell]) \nu_n^* \right) \\ & \times \mathbf{C}_{\eta}^{-1/2, *} \mathbf{T}[\ell] \mathbf{s}^{\text{UL}}[\ell] + \mathbf{G}[\ell] \mathbf{n}[\ell], \quad (38) \end{aligned}$$

with  $\mathbf{E}_{\text{B}}^*[\ell] = [\mathbf{E}_{\text{B}, 1}^*[\ell], \dots, \mathbf{E}_{\text{B}, K}^*[\ell]] \in \mathbb{C}^{N_t \times N_r K}$  and  $\mathbf{E}_{e, n}^*[\ell] = [\mathbf{E}_{e, 1, n}^*[\ell], \dots, \mathbf{E}_{e, K, n}^*[\ell]] \in \mathbb{C}^{N_t \times N_r K}$ ,  $\hat{\mathbf{H}}_{e, n}^*[\ell] = [\hat{\mathbf{H}}_{e, 1, n}^*[\ell], \dots, \hat{\mathbf{H}}_{e, K, n}^*[\ell]] \in \mathbb{C}^{N_t \times N_r K}$ ,  $\forall n$ . The MMSE receive filter using this compact formulation is given by

$$\begin{aligned} \mathbf{G}_{\text{MMSE}}[\ell] = & \mathbf{T}^*[\ell] \mathbf{C}_{\eta}^{-1/2} \hat{\mathbf{H}}_{e, k}[\ell] \\ & \times \left( \hat{\mathbf{H}}_e^*[\ell] \mathbf{C}_{\eta}^{-1/2, *} \mathbf{T}[\ell] \mathbf{T}^*[\ell] \mathbf{C}_{\eta}^{-1/2} \hat{\mathbf{H}}_e[\ell] + \mathbf{I}_{N_t} \right. \\ & \left. + (1+N) \sum_{i=1}^K \text{tr} \left( \frac{L}{P_T} \mathbf{T}_i[\ell] \mathbf{T}_i^*[\ell] \right) \mathbf{I}_{N_t} \right)^{-1}, \quad (39) \end{aligned}$$

and the overall uplink MSE achieved at subcarrier  $\ell$  when employing this MMSE receiving filter is

$$\begin{aligned} \text{MSE}^{\text{UL}}[\ell] = & \text{tr} \left[ \left( \mathbf{I}_{N_s[\ell]} + \mathbf{T}^*[\ell] \mathbf{C}_{\eta}^{-1/2} \hat{\mathbf{H}}_e[\ell] \right. \right. \\ & \times \left( \mathbf{I}_{N_t} + (1+N) \sum_{i=1}^K \text{tr} \left( \frac{L}{P_T} \mathbf{T}_i[\ell] \mathbf{T}_i^*[\ell] \right) \mathbf{I}_{N_t} \right)^{-1} \\ & \left. \left. \times \hat{\mathbf{H}}_e^*[\ell] \mathbf{C}_{\eta}^{-1/2, *} \mathbf{T}[\ell] \right)^{-1} \right]. \quad (40) \end{aligned}$$

According to [46, 47], the filters and precoders in the downlink are simply related to their counterparts in the dual MAC as follows:

$$\mathbf{P}[\ell] = \xi[\ell] \mathbf{G}^*[\ell], \quad (41)$$

$$\mathbf{W}[\ell] = \xi^{-1}[\ell] \mathbf{T}^*[\ell] \mathbf{C}_{\eta}^{-1/2}, \quad (42)$$

with  $\xi[\ell] \in \mathbb{R}$ , given by

$$\xi[\ell] = \sqrt{\frac{P_T[\ell]}{\sum_{k=1}^K \|\mathbf{G}_k[\ell]\|_F^2}}, \quad (43)$$

where  $P_T[\ell]$  is the power allocated at subcarrier  $\ell$ . On the other hand, the MAC-BC dual relationship can be easily established as

$$\mathbf{G}[\ell] = \zeta^{-1}[\ell] \mathbf{P}^*[\ell], \quad (44)$$

$$\mathbf{T}[\ell] = \mathbf{C}_{\eta}^{-1/2, *} \mathbf{W}^*[\ell] \zeta[\ell], \quad (45)$$

with  $\zeta[\ell] \in \mathbb{R}$  given by

$$\zeta[\ell] = \sqrt{\frac{P_T[\ell]}{\sum_{k=1}^K \|\mathbf{W}_k[\ell]\|_F^2}}. \quad (46)$$

Because of duality, the same sum-MSE is achieved in the downlink when using (41) and (42) to obtain the wideband downlink precoders and filters from the wideband uplink filters and precoders. Table III summarizes the main system model parameters and variables for the dual MAC system.

TABLE III  
 DUAL MAC SYSTEM MODEL PARAMETERS.

Parameter	Setting
Precoder of $k$ -th user at subcarrier $\ell$	$\mathbf{T}_k[\ell]$
(BC-MAC) frequency flat IRS phase shift matrix	$\Theta^*$
User-BS direct channel of $k$ -th user at subcarrier $\ell$	$\mathbf{H}_{\text{B},k}^*[\ell]\mathbf{C}_\eta^{-1/2,*}$
BS-IRS channel at subcarrier $\ell$	$\mathbf{H}_{\text{BI}}^*[\ell]$
IRS-User channel of $k$ -th user at subcarrier $\ell$	$\mathbf{H}_{\text{I},k}^*[\ell]\mathbf{C}_\eta^{-1/2,*}$
Vector of AWGN at subcarrier $\ell$	$\mathbf{n}[\ell]$
$k$ -th BS equalizer filter at subcarrier $\ell$	$\mathbf{G}_k[\ell]$
Vector of $N_{s,k}[\ell]$ estimated symbols at subcarrier $\ell$	$\hat{\mathbf{s}}_k^{\text{UL}}[\ell]$

Once the uplink MSE corresponding to all the  $K$  users for a particular subcarrier has been determined, we can similarly define  $\text{MSE}^{\text{UL}} = \sum_{\ell=1}^L \text{MSE}^{\text{UL}}[\ell] = \sum_{k=1}^K \sum_{\ell=1}^L \text{MSE}_k^{\text{UL}}[\ell]$  which is the overall system MSE in the dual uplink when considering the symbols transmitted by all the users over all the subcarriers. This uplink MSE can be represented in a compact form as follows

$$\text{MSE}^{\text{UL}} = \text{tr} \left[ \left( \mathbf{I}_{N_s L} + \mathbf{T}^* \mathbf{C}^{-1/2} \hat{\mathbf{H}}_e \left( \mathbf{I}_L \otimes \mathbf{I}_{N_t} + (1 + N) \times \frac{L}{P_T} \|\mathbf{T}\|_{\text{F}}^2 \mathbf{I}_{N_s L} \right)^{-1} \hat{\mathbf{H}}_e^* \mathbf{C}^{-1/2,*} \mathbf{T} \right)^{-1} \right], \quad (47)$$

where  $\mathbf{I}_{N_s L}$  is the  $N_s L \times N_s L$  identity matrix and

$$\hat{\mathbf{H}}_e = \hat{\mathbf{H}}_B + \sum_{n=1}^N \tilde{\nu}_n \hat{\mathbf{H}}_{c,n}, \quad (48)$$

where  $\tilde{\nu}$  is the main diagonal of the resulting matrix after applying  $\hat{\Theta} = \mathbf{I}_L \otimes \Theta$  and

$$\begin{aligned} \mathbf{T}^* &= \text{blkdiag}(\mathbf{T}^*[1], \dots, \mathbf{T}^*[L]), \quad \mathbf{C} = \mathbf{I}_L \otimes \mathbf{C}_\eta, \\ \hat{\mathbf{H}}_B^* &= \text{blkdiag}(\hat{\mathbf{H}}_B^*[1], \dots, \hat{\mathbf{H}}_B^*[L]), \\ \mathbf{E}_B^* &= \text{blkdiag}(\mathbf{E}_B^*[1], \dots, \mathbf{E}_B^*[L]), \\ \mathbf{E}_{c,n}^* &= \text{blkdiag}(\mathbf{E}_{c,n}^*[1], \dots, \mathbf{E}_{c,n}^*[L]), \quad \forall n = 1, \dots, N, \\ \hat{\mathbf{H}}_{c,n}^* &= \text{blkdiag}(\hat{\mathbf{H}}_{c,n}^*[1], \dots, \hat{\mathbf{H}}_{c,n}^*[L]), \quad \forall n = 1, \dots, N \end{aligned}$$

are block diagonal matrices that stack all the precoders, the noise covariance matrices and the channel responses corresponding to the  $K$  users at the  $L$  subcarriers, such that  $\mathbf{T} \in \mathbb{C}^{N_t K L \times N_s}$ ,  $\hat{\mathbf{H}}_{c,n}^* \in \mathbb{C}^{N_t K L \times N_s L}$ ,  $\mathbf{H}_B^* \in \mathbb{C}^{N_t K L \times N_s L}$ ,  $\mathbf{E}_B^* \in \mathbb{C}^{N_t K L \times N_s L}$  and  $\mathbf{E}_{c,n}^* \in \mathbb{C}^{N_t K L \times N_s L}$ .

Using the previous compact notation, the MMSE optimization problem for the virtual uplink can be formulated as follows

$$\begin{aligned} \arg \min_{\Theta, \mathbf{T}_k[\ell], \forall k, \ell} \quad & \text{MSE}^{\text{UL}}(\mathbf{T}, \Theta) \\ \text{s.t.} \quad & \sum_{k=1}^K \text{tr}(\mathbf{T}_k[\ell] \mathbf{T}_k^*[\ell]) \leq P_T[\ell], \quad \forall \ell, \quad \Theta \in \mathcal{D}, \end{aligned} \quad (49)$$

with  $\text{MSE}^{\text{UL}}$  given in (47). Note that after obtaining the precoders  $\mathbf{T}_k[\ell] \forall k, \ell$  and the receiving filters  $\mathbf{G}_{\text{MMSE},k}[\ell] \forall k, \ell$  in the dual uplink, we readily determine  $\mathbf{P}_k[\ell] \forall k, \ell$  and  $\mathbf{W}_{\text{MMSE},k}[\ell] \forall k, \ell$  in the downlink by means of (41) and the MMSE expression in (23), respectively.

### A. Alternating MSE minimization algorithm

In this subsection, we develop an alternating algorithm to solve the MSE minimization problem (49). The frequency-flat IRS phase-shift matrix  $\Theta$  and the frequency-dependent filters/precoders in the uplink and their downlink counterparts are alternately calculated until the MSE reduction is not higher than a threshold  $\delta$  or until a maximum number of iterations  $\epsilon$  is reached.

Algorithm 1 summarizes the steps of the proposed alternating minimization approach. Algorithm 1 starts determining the filters and downlink precoders, which are next used to determine the filters and precoders in the dual uplink through (45) and (39). Then, the IRS phase shift matrix  $\Theta = \text{diag}(\boldsymbol{\nu})$  is determined with the following iterative projected gradient algorithm

$$\boldsymbol{\nu}^{(i)} = d \left( \boldsymbol{\nu}^{(i-1)} - \mu_{\boldsymbol{\nu}} \nabla_{\boldsymbol{\nu}} \text{MSE}^{\text{UL}}(\mathbf{T}^{(i)}, \boldsymbol{\nu}^{(i)}) \right). \quad (50)$$

The operator  $d(\cdot)$  is a projector which enforces  $\nu_n, \forall n$  to be a unitary modulus element and, thus,  $\Theta$  to belong to the set of feasible solutions  $\mathcal{D}$ , i.e.,  $d(\cdot)$  ensures that the IRS matrix is diagonal with unit magnitude entries. Next, the MAC-BC duality expression in (41) and the MMSE filter expression in (23) are used to compute the precoders and filters in the downlink, i.e.,  $\mathbf{P}_k[\ell] \forall k, \ell$  and  $\mathbf{W}_{\text{MMSE},k}[\ell] \forall k, \ell$ , respectively. By invoking the MAC-BC duality in both directions, this alternating procedure is repeated until achieving the stopping criterion in line 21.

The initial IRS phase-shift matrix  $\Theta^{(0)}$  is set to a diagonal matrix whose non-zero entries have unit magnitude and a random phase from the interval  $[0, 2\pi)$  (line 3). The initial block diagonal precoding matrix in the downlink  $\mathbf{P}^{(0)}$  is constructed with the maximum ratio transmitter (MRT) precoders for each user at each subcarrier (line 5) assuming the uniform power allocation  $P_{\text{T}k}[\ell] = \frac{P_T}{KL} \forall k, \ell$ . Notice that Algorithm 1 also updates at each iteration the power allocation per user and per subcarrier.

Considering

$$\mathbf{B}(\boldsymbol{\nu}) = \mathbf{I}_{N_s L} + \mathbf{T}^* \mathbf{C}^{-1/2} \mathbf{H}_e \mathbf{H}_e^* \mathbf{C}^{-1/2,*} \mathbf{T} \frac{1}{1 + (N+1) \frac{L}{P_T} \|\mathbf{T}\|_{\text{F}}^2}$$

and  $\text{MSE}^{\text{UL}}(\mathbf{T}, \boldsymbol{\nu}) = \text{tr}[\mathbf{B}^{-1}(\boldsymbol{\nu})]$ , we get the gradient  $\nabla_{\boldsymbol{\nu}_n} \text{MSE}^{\text{UL}}(\mathbf{T}, \boldsymbol{\nu})$  used in (50)

$$\begin{aligned} \nabla_{\boldsymbol{\nu}_n} \text{MSE}^{\text{UL}}(\mathbf{T}, \boldsymbol{\nu}) &= -\text{tr} \left( \mathbf{B}^{-2}(\boldsymbol{\nu}) \mathbf{T}^* \mathbf{C}^{-1/2} \hat{\mathbf{H}}_{c,n} \hat{\mathbf{H}}_{c,n}^* \mathbf{C}^{-1/2,*} \mathbf{T} \right) \\ &\times \frac{1}{1 + (1+N) \frac{L}{P_T} \|\mathbf{T}\|_{\text{F}}^2}, \end{aligned} \quad (51)$$

where we have used the equality  $\nabla_{\beta} \text{tr}(\mathbf{A}^{-1}(\beta)) = -\text{tr}(\mathbf{A}^{-2}(\beta)) \frac{\partial \mathbf{A}(\beta)}{\partial \beta}$ .

### V. CONVERGENCE ANALYSIS

In this section, we conduct an analysis of the convergence properties of the proposed alternating MSE minimization PG algorithm. Algorithm 1 iterates over the precoders/filters (in both the BC and the dual MAC system) for the  $L$  subcarriers, as well as on the diagonal elements of the frequency-flat IRS

---

**Algorithm 1** Alternating MSE Minimization PG
 

---

**Input:**  $\mathbf{C}_{\eta_k}, \forall k, P_T, \mu_1, \delta, \epsilon, \hat{\mathbf{H}}_B^* \in \mathbb{C}^{LN_r K \times LN_t}, \hat{\mathbf{H}}_{c,n}^* \in \mathbb{C}^{LN_r K \times LN_t}, \forall n$

```

1: Initialize:  $i \leftarrow 0$ 
2:  $\theta_n \in [0, 2\pi), \forall n$ 
3:  $\Theta^{(0)} = \text{diag}(e^{j\theta_1}, \dots, e^{j\theta_N}), \forall n$ 
4: for  $\ell = 1 : L$  do
5:    $\mathbf{P}^{(0)}[\ell] = [\mathbf{P}_1^{(0)}[\ell], \dots, \mathbf{P}_K^{(0)}[\ell]] \leftarrow$  MRT precoders
6:    $\mathbf{W}_{\text{MMSE}}^{(0)}[\ell] = \text{blkdiag}(\mathbf{W}_{\text{MMSE},1}^{(0)}[\ell], \dots, \mathbf{W}_{\text{MMSE},K}^{(0)}[\ell]) \leftarrow$  (23)
7:    $\mathbf{T}^{(0)}[\ell] = \text{blkdiag}(\mathbf{T}_1^{(0)}[\ell], \dots, \mathbf{T}_K^{(0)}[\ell]) \leftarrow$  (45)
8:    $\mathbf{G}_{\text{MMSE}}^{(0)}[\ell] = [\mathbf{G}_{\text{MMSE},1}^{*(0)}[\ell], \dots, \mathbf{G}_{\text{MMSE},K}^{*(0)}[\ell]]^* \leftarrow$  (39)
9:    $\mu_\Theta \leftarrow \mu_1$ 
10: repeat
11:    $i \leftarrow i + 1$ 
12:   for  $\ell = 1 : L$  do
13:      $\mathbf{P}^{(i)}[\ell] = [\mathbf{P}_1^{(i)}[\ell], \dots, \mathbf{P}_K^{(i)}[\ell]] \leftarrow$  (41) and  $\mathbf{G}_k^{(i-1)}[\ell]$ 
14:      $\mathbf{W}_{\text{MMSE}}^{(i)}[\ell] = \text{blkdiag}(\mathbf{W}_{\text{MMSE},1}^{(i)}[\ell], \dots, \mathbf{W}_{\text{MMSE},K}^{(i)}[\ell]) \leftarrow$  (23)
15:      $\mathbf{T}^{(i)}[\ell] = \text{blkdiag}(\mathbf{T}_1^{(i)}[\ell], \dots, \mathbf{T}_K^{(i)}[\ell]) \leftarrow$  (45)
16:      $\mathbf{G}_{\text{MMSE}}^{(i)}[\ell] = [\mathbf{G}_{\text{MMSE},1}^{*(i)}[\ell], \dots, \mathbf{G}_{\text{MMSE},K}^{*(i)}[\ell]]^* \leftarrow$  (39)
17:      $\nu^{(i)} = d(\nu^{(i-1)} - \mu_\nu \nabla_\nu \text{MSE}^{\text{UL}}(\mathbf{T}^{(i)}, \nu^{(i)}))$ 
18:     while  $\text{MSE}^{\text{UL}}(\mathbf{T}^{(i-1)}, \nu^{(i-1)}) \leq \text{MSE}^{\text{UL}}(\mathbf{T}^{(i)}, \nu^{(i)})$  do
19:        $\mu_\nu \leftarrow \mu_\nu / 2$ 
20:        $\nu^{(i)} = d(\nu^{(i-1)} - \mu_\nu \nabla_\nu \text{MSE}^{\text{UL}}(\mathbf{T}^{(i)}, \nu^{(i)}))$ 
21: until  $\text{MSE}^{\text{UL}}(\mathbf{T}^{(i-1)}, \nu^{(i-1)}) - \text{MSE}^{\text{UL}}(\mathbf{T}^{(i)}, \nu^{(i)}) < \delta$  or  $i \geq \epsilon$ 

```

**Output:**  $\mathbf{P}_k[\ell], \mathbf{W}_{\text{MMSE},k}[\ell], \forall k, \ell, \Theta \in \mathcal{D}$

---

phase-shift matrix. At each iteration, the algorithm produces  $\mathbf{P}^{(i)}[\ell], \mathbf{W}_{\text{MMSE}}^{(i)}[\ell], \mathbf{T}^{(i)}[\ell], \mathbf{G}_{\text{MMSE}}^{(i)}[\ell]$  and  $\nu^{(i)}$ .

The precoders/filters for each subcarrier with  $\ell = 1, \dots, L$  in both the BC and the dual MAC system are obtained using the MSE dualities as explained in Section IV-A. Initially, the precoders  $\mathbf{P}^{(0)}[\ell]$  in the BC are obtained via MRT precoding, while the closed-form expression in equation (23) is used to compute the MMSE filters  $\mathbf{W}_{\text{MMSE}}^{(0)}[\ell]$  in the BC. Next, the precoders  $\mathbf{T}^{(0)}[\ell]$  in the dual MAC system are computed using the BC-MAC duality given by (45), and the closed-form expression in (39) is employed to obtain the MAC MMSE filters  $\mathbf{G}_{\text{MMSE}}^{(0)}[\ell]$ . After these initialization operations, during the  $i$ -th iteration, the precoders  $\mathbf{P}^{(i)}[\ell]$  are computed using the MAC-BC duality as expressed in (41), and the filters  $\mathbf{W}_{\text{MMSE}}^{(i)}[\ell]$  are obtained through the closed-form expression in (21). Additionally, the MAC precoders  $\mathbf{T}^{(i)}[\ell], \forall \ell$  and the MAC filters  $\mathbf{G}_{\text{MMSE}}^{(i)}[\ell], \forall \ell$  are once again obtained using the BC-MAC duality in (45) and the closed-form expression in (39), respectively. The IRS phase shift matrix  $\Theta = \text{diag}(\nu)$  is determined by using the gradient  $\nabla_\nu \text{MSE}^{\text{UL}}(\mathbf{T}, \nu)$  as described in (50).

To prove convergence, it is sufficient to ensure that the performance metric  $\text{MSE}^{\text{UL}}(\mathbf{T}^{(i)}, \nu^{(i)})$  either decreases or remains constant at each iteration. Since the performance

metric is lower bounded, this property guarantees that the proposed algorithm converges to a local optimum. Hence, we need to verify that each sequence  $\{\text{MSE}^{\text{UL}}(\mathbf{T}, \nu^{(i)})\}$  and  $\{\text{MSE}^{\text{UL}}(\underline{\mathbf{T}}^{(i)}, \nu^{(i)})\}$  converges to a local minimum, where  $\underline{\mathbf{X}}$  denotes the fixed variables.

1) *Convergence of the sequences  $\{\text{MSE}^{\text{UL}}(\mathbf{T}, \nu^{(i)})\}$ :* The convergence of the MSE duality procedure in conventional communication systems without IRSs (or a fixed IRS) has been previously analyzed. In [48] (please, see Sections III and IV), the authors prove monotonic convergence, and it is observed that the algorithm converges rapidly in the initial iterations. However, proving global optimality is challenging. In this case, for Algorithm 1, the sequences produced  $\{\text{MSE}^{\text{UL}}(\mathbf{T}^{(i)}, \nu^{(i)})\}$  converge to a local minimum. However, this assumption is based on a fixed  $\Theta = \text{diag}(\nu)$ . In our implementation, we update  $\nu^{(i)}$  for the  $i$ -th iteration within expressions (23) and (39) in  $\hat{\mathbf{H}}_c[\ell]$  (cf. (12)). As a result, it becomes crucial to ensure the convergence of the sequences  $\{\text{MSE}^{\text{UL}}(\underline{\mathbf{T}}^{(i)}, \nu^{(i)})\}$  for a given or fixed precoder  $\mathbf{T}$ .

2) *Convergence of the sequences  $\{\text{MSE}^{\text{UL}}(\underline{\mathbf{T}}^{(i)}, \tilde{\nu}^{(i)})\}$ :* Let us define the auxiliary IRS phase-shift matrix as follows

$$\tilde{\nu}^{(i)} = \tilde{\nu}^{(i-1)} - \mu_\nu \nabla_\nu \text{MSE}^{\text{UL}}(\mathbf{T}^{(i)}, \tilde{\nu}^{(i)})$$

at the  $\ell$ -th iteration, where  $\tilde{\nu}$  represents the unconstrained solution for the optimization problem in (49). Note that  $\mathbf{T}$  and  $\tilde{\nu}$  are obtained in steps 15 and 17 of Algorithm 1, respectively, by neglecting the projection operator  $d(\cdot)$  for the IRS design. In this case, the sum-MSE sequences produced by the alternating minimization algorithm,  $\{\text{MSE}^{\text{UL}}(\mathbf{T}^{(i)}, \tilde{\nu})\}$  and  $\{\text{MSE}^{\text{UL}}(\underline{\mathbf{T}}, \tilde{\nu}^{(i)})\}$  converge to a local minimum with the proper adjustment of the step size  $\mu_\nu$ , and by using a line or Armijo's search [49]. To obtain  $\Theta = \text{diag}(\nu)$  within the feasible set  $\mathcal{D}$ , we employ the projector  $d(\cdot)$ , leading to the sequence  $\{\text{MSE}^{\text{UL}}(\underline{\mathbf{T}}, \nu^{(i)})\}$ . Hence, we need to verify that this sequence with constrained solutions converges to a local minimum, as we do next.

3) *Convergence of the sequences  $\{\text{MSE}^{\text{UL}}(\underline{\mathbf{T}}^{(i)}, \nu^{(i)})\}$ :* The projector  $d(\cdot)$  is employed to map  $\tilde{\nu}$  and obtain  $\Theta$  onto the non-convex set  $\mathcal{D}$ , i.e.,  $\Theta = \text{diag}(\nu)$ . Note that the unit modulus constraint defines a Riemannian manifold (cf. [50] and [51]), which is intrinsically non-convex. Nevertheless, it has been proven in [52] that if the function  $\text{MSE}^{\text{UL}}(\mathbf{T}, \nu)$  is differentiable with a continuous gradient, the convergence of  $\{\text{MSE}^{\text{UL}}(\underline{\mathbf{T}}, \nu^{(i)})\}$  to  $(\underline{\mathbf{T}}, \nu^{(0)})$  is ensured because  $\mathcal{D}$  is a compact set (see [52, Theorem 1] and [53, Appendix]).

Finally, it is essential to highlight that our approach based on alternating minimization over the individual variables provides a  $q$ -linear convergence rate over both  $\mathbf{T}$  and  $\nu$  under practical assumptions. Let  $(\mathbf{T}^{(0)}, \nu^{(0)})$  be the local minimum of  $\text{MSE}^{\text{UL}}(\mathbf{T}, \nu)$  on a neighborhood  $\mathcal{N}$  of  $(\mathbf{T}^{(0)}, \nu^{(0)})$  over which the function  $\text{MSE}^{\text{UL}}(\cdot)$  is convex. Given that  $\text{MSE}^{\text{UL}}(\mathbf{T}, \nu)$  is a smooth function (i.e., continuous and differentiable) over such  $\mathcal{N}$ , and taking into account that the Hessian matrix of  $\text{MSE}^{\text{UL}}(\cdot)$  is positive definite, alternating minimization over each variable ensures a  $q$ -linear convergence rate to  $(\mathbf{T}^{(0)}, \nu^{(0)})$  [54]. This condition holds when all the available channel spatial degrees of freedom are utilized, i.e., for mid-to-high SNR levels. This regime is practical for some IRS-

aided scenarios. The empirical verification of these findings is presented in the numerical results.

### VI. COMPUTATIONAL COMPLEXITY ANALYSIS

In this section, we analyze the computational complexity of Algorithm 1. The complexity orders for the main steps are summarized in Table IV. As shown, the complexity of step 5 (computation of MRT precoders) is bounded by  $\mathcal{O}(N_r N_t^2 KL)$  since  $KL$  singular value decompositions (SVDs) are necessary. In step 17 (update of  $\nu^{(i)}$ ), the gradient given by (51) is used and its computational complexity order is bounded by  $\mathcal{O}(LN_r N_t KN\epsilon)$ . Note that this line is performed  $\epsilon$  times at most. The complexity order of lines 18 and 20 used to compute the MSE performance metric (47) is  $\mathcal{O}(LN_r N_t KN\epsilon)$ . We conclude that Algorithm 1 leads to an overall complexity order of  $\mathcal{O}(N_r N_t^2 KL)$ .

TABLE IV  
COMPUTATIONAL COMPLEXITY OF ALGORITHM 1.

Operation	Num. of operations	Complexity order
Compute MRT Precoders (step 5)	1	$\mathcal{O}(N_r N_t^2 KL)$
Compute $\nu^{(i)}$ (step 17)	$\epsilon$	$\mathcal{O}(LN_r N_t KN\epsilon)$
Overall MSE evaluation (steps 18 and 20)	$\epsilon$	$\mathcal{O}(LN_r N_t KN\epsilon)$
<b>Overall</b>		$\mathcal{O}(N_r N_t^2 KL)$

### VII. SIMULATION RESULTS

In this section, we present the results of computer simulations carried out to assess the performance of the wideband IRS-aided MU MIMO system designed with the alternating MSE minimization algorithm proposed in Section IV. We consider a wideband IRS-aided MU MIMO system with  $K = 3$  users having  $N_r = 4$  antennas each,  $L = 32$  subcarriers, a BS with  $N_t = 9$  antennas which allocates 2 data streams per user at subcarrier  $\ell$ , i.e.,  $N_{s,k}[\ell] = 2 \forall k, \ell$ , and an IRS with different numbers of elements  $N \in \{9, 16, 25, 36, 49, 64, 81, 100\}$ . Although some authors assume that the estimation error level at the receivers is lower or even negligible, our approach is more general and can be adapted to those cases. The parameters of the mmWave channel model are set to  $L_D = 8$  delay taps,  $N_{\text{path}_B}$  channel paths for the BS-IRS links and  $N_{\text{path}_I}$  paths for the IRS-users links, respectively. The AoAs and the AoDs are assumed to be random and uniformly distributed over the interval  $[0, \pi]$  as in [55]. The relative delays  $\tau_n$  are also random and uniformly distributed over the range  $\tau_n \in [0, (L_D - 1)T_s]$ , with  $T_s = 1/f_s$  and  $f_s = 1760$  MHz. The complex-valued channel gains are i.i.d. standard Gaussian random variables, i.e.,  $\beta_m \sim \mathcal{N}_C(0, 1)$ . The central carrier frequency is assumed to be  $f_c = 28$  GHz and the signal bandwidth is set to 400 MHz.

All the reported results are obtained after averaging  $C_R = 1000$  channel realizations. Performance is evaluated in terms of the downlink achievable sum-rate (17) and the MSE between the transmitted and estimated symbols. We assume that the noise covariance matrix has the form  $\mathbf{C}_{\eta_k} = \sigma_{\eta_k}^2 \mathbf{I}$ , with equal noise power for the noise during data transmission and training stages, i.e.,  $\sigma_{\eta_k}^2 = \sigma_{\eta}^2 = 1 \forall k$ . Therefore, the

per subcarrier signal-to-noise ratio is given by  $\text{SNR} (\text{dB}) = 10 \log_{10}(P_T/L)$ . The channel responses of the direct and cascaded channels are assumed to be imperfectly known, following a stochastic model where  $\mathbf{E}_{B,k}[\ell]$  and  $\mathbf{E}_{c,k,n}[\ell]$  are assumed to follow a complex Gaussian distribution  $\mathcal{N}_C(\mathbf{0}, \frac{L}{P_T} \mathbf{C}_{\eta_k})$ , similar to the approaches in [56, 57]. Note that this assumption entails a lower estimation error while the SNR increases. Finally, the maximum number of iterations  $\epsilon$  in Algorithm 1 is set to 100. Table V summarizes the system model configuration considered in the computer simulations.

TABLE V  
SIMULATION PARAMETER SETTING.

Parameter	Setting
Number of users	$K = 3$
Antennas per users	$N_r = 4$
Antennas at the BS	$N_t = 16$
Number of subcarriers	$L = 32$
Number of data streams per user	$N_{s,k}[\ell] = 2, \forall k, \ell$
Number of IRS elements	$N \in \{9 \sim 144\}$
BS-IRS channel propagation paths	$N_{\text{path}_B} = 4$
IRS-users channel propagation paths	$N_{\text{path}_I} \in \{2, 3, 4\}$
Channel delay paths	$L_D = 8$
Central carrier frequency	$f_c = 28$ GHz
Covariance of estimation error (downlink)	$\frac{L}{P_T} \mathbf{C}_{\eta_k}, \forall k$
Channel realizations	$C_R = 1000$
Max. number of iterations (Algorithm 1)	$\epsilon = 100$

In the first simulation experiment, we compare the performance of the system designed according to Algorithm 1 with the following five baseline approaches:

- 1) The maximum achievable sum-capacity obtained by assuming dirty paper coding (DPC) and optimizing the IRS. This approach constitutes an upper bound on the sum-rate and has been designed with the power iterative waterfilling algorithm proposed in [58, Algorithm 2]. In this approach, we obtain the precoders for both the downlink and uplink systems using the iterative waterfilling algorithm presented in [58]. Meanwhile, the IRS phase shift matrix is updated at each iteration by following Algorithm 1. Note that this scheme yields the sum-capacity of the system for each equivalent channel  $\mathbf{H}_e[\ell]$  provided by the IRS setup at each step. This is achieved by configuring the optimal precoders (optimal transmit policies) via DPC under perfect CSI.
- 2) Amplify-and-Forward with optimized precoders (AF O-PS). The precoders and the IRS matrix are optimized through Algorithm 1 but the IRS matrix is assumed to be unconstrained, i.e., the magnitude of the diagonal entries of the phase-shift matrix is not constrained to be 1, and thus the IRS is able to modify both the amplitude and the phase of the impinging signals. For the sake of fairness, we assume that  $\|\Theta\|_F^2 = N$ . This strategy is employed as an alternative upper bound for the design of the IRS phase shift matrix, given that achieving a globally optimal solution requires the use of the exhaustive search technique, which is computationally impractical, even for a system of moderate size.

- 3) Random IRS with optimized precoders (R-IRS O-Ps). The precoders are optimized via the MAC-BC and the BC-MAC dualities in Algorithm 1 while the phases of the diagonal IRS phase-shift matrix are random uniform variables over  $[0, 2\pi]$ , i.e., there is no control of the IRS phase-shift matrix.
- 4) Optimized IRS with MRT precoders (O-IRS MRT-Ps). The precoders are designed as MRT precoders while the IRS phase-shift matrix is optimized via Algorithm 1.
- 5) No IRS with MRT precoders (No-IRS MRT-Ps). The precoders are designed as MRT precoders and the IRS is not deployed to assist the communication system, i.e.,  $\Theta = \mathbf{0}$ . Only the direct link between the BS and the users is available.

In all the considered approaches (the proposed one and the five baselines), the wideband receiving filters  $\mathbf{W}_k[\ell] \forall \ell, k$  are designed according to the MMSE criterion. It is also worth remarking that perfect CSI is assumed in this first experiment. Note that the MMSE expressions are readily adapted to perfect CSI by setting the error covariance matrix to  $\mathbf{0}$ .

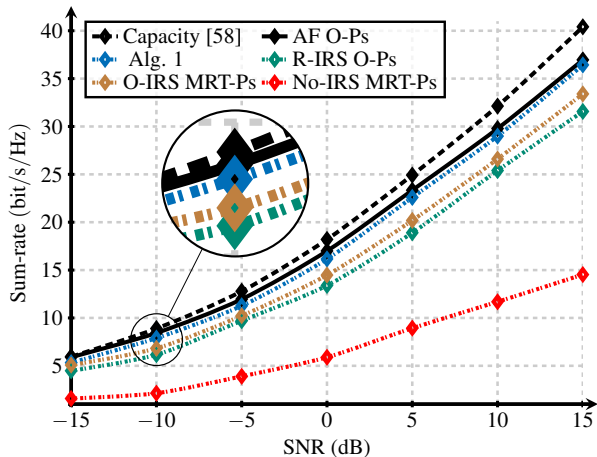


Fig. 4. Sum-rate (bit/s/Hz) vs SNR (dB) for  $K = 3$  users,  $N_r = 4$ ,  $N_t = 9$ ,  $L = 32$ ,  $N = 25$ , and  $N_{s,k}[\ell] = 2, \forall k, \ell$ .

Fig. 4 plots the achievable sum-rate obtained with the above mentioned approaches. As shown, AF O-Ps provides the highest achievable sum-rate since the wideband precoders are optimized via Algorithm 1 and the IRS phase-shift matrix entries have no magnitude constraint. The proposed PG-based approach leads to a performance higher than that obtained with the R-IRS O-Ps and the O-IRS MRT-Ps baseline approaches. Recall that R-IRS O-Ps does not optimize the IRS phases while O-IRS MRT-Ps does not account for the interference when designing the BS wideband precoders. The No-IRS MRT-Ps strategy provides the lowest system performance because only the direct channel is available. Thus, the system has a reduced capacity and the wideband precoder design does not take into account the MU interference. It is also observed that the proposed PG approach via Algorithm 1 does not lead to a significant gap w.r.t. the unconstrained AF O-Ps strategy and comes close to the maximum system capacity. Hence, the obtained results are very appealing because the proposed design algorithm is able to efficiently

exploit the deployment of a passive IRS to improve the system performance.

From Fig. 4, we can clearly observe a significant gain provided by the PG-based approach over the No-IRS MRT-Ps strategy, representing the improvement brought about by the IRS in enhancing the system performance. However, this gain is influenced by the quality of the channels between the IRS and the users, which is determined by the positioning of the IRS in practical deployment scenarios. Thus far we have considered  $N_{\text{path}_B} = N_{\text{path}_I} = 4$ . In Table VI, we define  $G_{\text{IRS}}$  (bit/s/Hz) as the difference between the achievable sum-rate of the PG-based approach and the No-IRS MRT-Ps strategy. We also vary the number of reflection paths in the channels between the IRS and the users ( $N_{\text{path}_I}$ ). As expected, the results demonstrate that the gains  $G_{\text{IRS}}$  (bit/s/Hz) decrease as the IRS-user links become weaker, indicating that the effectiveness of the IRS is closely related to the quality of these channels.

TABLE VI  
 $G_{\text{IRS}}$  (BIT/S/Hz) FOR DIFFERENT IRS-USER CHANNEL CONDITIONS.

Num. of paths	5 dB	10 dB	15 dB
$N_{\text{path}_I} = 2$	2.87	6.55	10.02
$N_{\text{path}_I} = 3$	10.75	14.52	18.31
$N_{\text{path}_I} = 4$	13.62	17.30	21.90

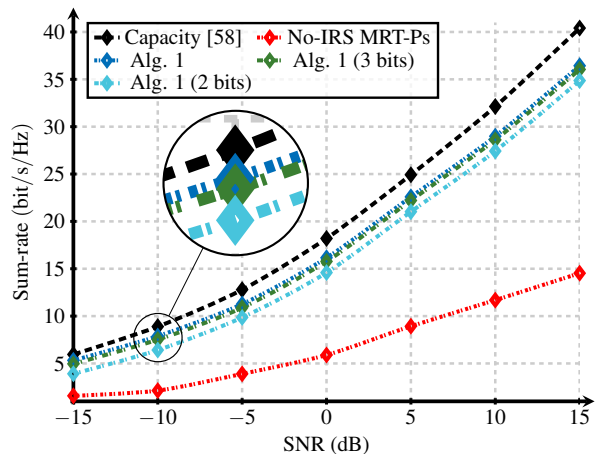


Fig. 5. Sum-rate (bit/s/Hz) vs SNR (dB) for  $K = 3$  users,  $N_r = 4$ ,  $N_t = 9$ ,  $L = 32$ ,  $N = 25$ ,  $N_{s,k}[\ell] = 2, \forall k, \ell$  and discrete phase shifts (2 and 3 bits).

We considered infinite resolution variable phase shifts to implement the IRS matrix. However, in practical scenarios, phase shifters are typically limited to a finite number of discrete values. To evaluate the impact of this quantization, we performed simulations for phase shift resolutions of 3 and 2 bits. The results in Fig. 5 show that the performance loss due to quantization is negligible when using IRS phase shifting matrices with 8 available phases (3 bits). On the other hand, for IRS phase shifting matrices with only 4 quantized values (2 bits), the performance loss is moderate.

In Fig. 6, we present the sum-rate for a specific setup with  $K = 3$  users,  $N_r = 4$ ,  $N_t = 9$ ,  $L = 32$ ,  $N = 25$ ,  $\text{SNR} = 10$  (dB), and  $N_{s,k}[\ell] = 2$  streams per user at subcarrier  $\ell$ . The continuous-valued IRS phase-shift matrix obtained via Algorithm 1 is used as the baseline for comparison. The figure shows that the sum-rate degradation due to discretizing the IRS

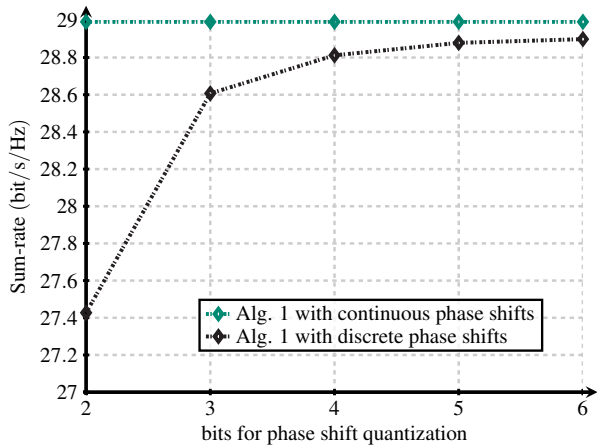


Fig. 6. Sum-rate (bit/s/Hz) vs. the number of bits used for phase-shift quantization levels for  $K = 3$  users,  $N_r = 4$ ,  $N_t = 9$ ,  $L = 32$ ,  $N = 25$ ,  $\text{SNR} = 10$  dB and  $N_{s,k}[\ell] = 2, \forall k, \ell$ .

phase shifts is lower than 2 bit/s/Hz, even when considering only 4 possible quantization phases (2 bits). Furthermore, this degradation effect steeply decreases when more bits are used for the phase-shift quantization.

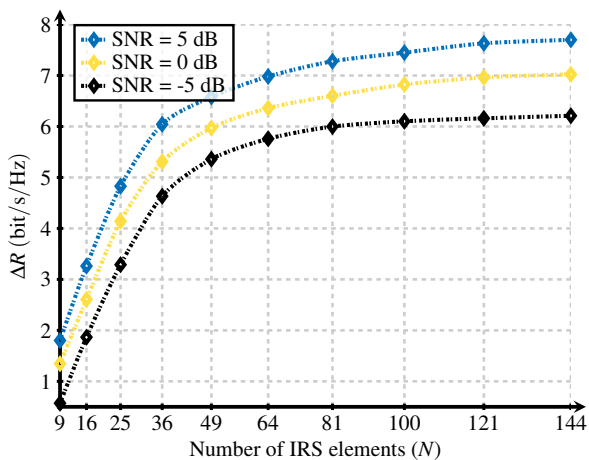


Fig. 7. Sum-rate increase  $\Delta R$  (bit/s/Hz) vs  $N$  for  $K = 3$  users,  $N_r = 4$ ,  $N_t = 9$ ,  $\text{SNR}$  (dB)  $\in \{-5, 0, 5\}$ ,  $L = 32$ ,  $N \in \{9, 16, 25, 36, 49, 64, 81, 100, 121, 144\}$ , and  $N_{s,k}[\ell] = 2, \forall k, \ell$ .

In the next experiment, we quantify the performance improvement obtained when optimizing the IRS phase-shift matrix with Algorithm 1. More specifically, we measure the impact of the phase-shift optimization at the IRS and evaluate the performance gains obtained when increasing the number of IRS elements  $N$ . For that, we define the achievable sum-rate increase  $\Delta R$  (bit/s/Hz) as the difference between the achievable sum-rate obtained with Algorithm 1 and that obtained with R-IRS O-Ps. The obtained results are presented in Fig. 7. As expected, the larger the size of the IRS is, the higher the resulting gains are. Fig. 7 also shows how  $\Delta R$  (bit/s/Hz) increases with SNR (dB). This effect is because of the optimization of the IRS phase-shift matrix and, therefore, the control of the MU interference has a larger impact on the system performance in the high SNR regime.

Another interesting observation from the results in the figure is the saturation of the performance gains  $\Delta R$ (bit/s/Hz)

beyond a certain number of IRS elements. This behavior is inherently linked to the specific  $N_r \times N_t$  MIMO wideband ( $L$  subcarriers) configuration adopted for the MU scheme with  $K$  users, as well as the considered channel rank for the simulations. The system setup will determine how much improvement a large number of IRS elements can provide to the communication system.

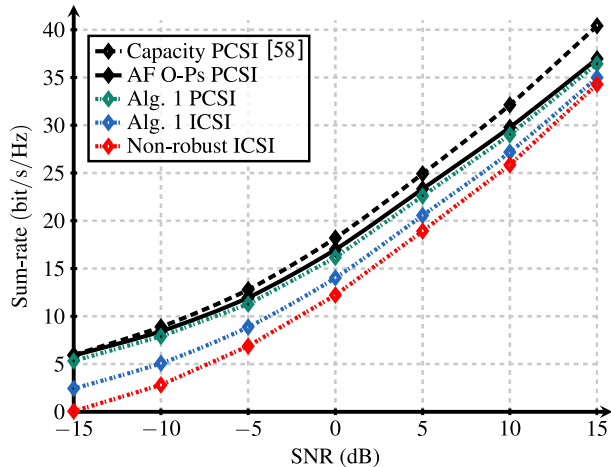


Fig. 8. Sum-rate (bit/s/Hz) vs SNR (dB) for  $K = 3$  users,  $N_r = 4$ ,  $N_t = 9$ ,  $N = 25$ ,  $L = 32$ , imperfect CSI, and  $N_{s,k}[\ell] = 2, \forall k, \ell$ .

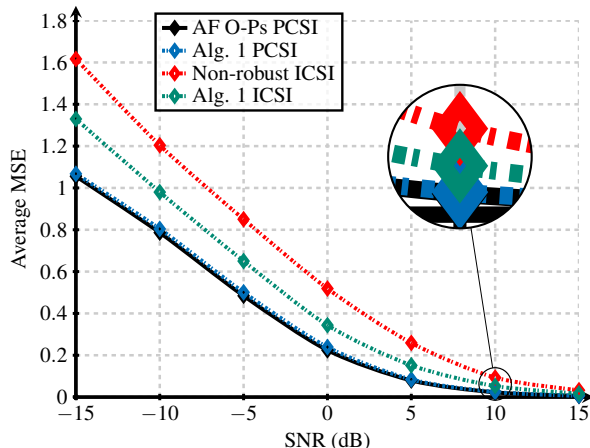


Fig. 9. Average MSE vs SNR (dB) for  $K = 3$  users,  $N_r = 4$ ,  $N_t = 9$ ,  $N = 25$ ,  $L = 32$ , imperfect CSI, and  $N_{s,k}[\ell] = 2, \forall k, \ell$ .

In the following, we evaluate (in terms of the achievable sum-rate) the impact of the CSI estimation errors and compare the proposed solution with a baseline (labeled non-robust) that does not take into account the uncertainty introduced by the imperfect CSI (Algorithm 1 in [59]). We also include an approach where the precoders and the IRS phase-shift matrix are determined with the proposed algorithm but assuming perfect CSI. Finally, we included the sum-capacity and the AF O-Ps solutions with perfect CSI as benchmarks.

As shown in Fig. 8, the non-robust strategy leads to the worst system performance since it does not consider imperfect CSI and neglects the knowledge about the error statistics. This behavior is more apparent in the low SNR regime, where the channel estimation errors are larger. Conversely, Algorithm 1 considers the error statistics in the estimation of the direct and the cascaded channels, and outperforms the non-robust approach leading to a decreasing gap w.r.t. the perfect

CSI. This decreasing gap is observed since the estimation errors decrease in the high SNR regime, and thus the system performance of the imperfect CSI scheme approaches that of the perfect CSI scenario. We remark that the behavior of the gap between the sum-rates achieved with the proposed solution in Algorithm 1 and with the non-robust strategy is influenced by the assumed covariance model for the errors, which leads to larger channel estimation errors in the low SNR regime. Nevertheless, our proposed solution in Algorithm 1 remains independent of the specific error model and the corresponding covariance matrix used for modeling the errors.

In Fig. 9, we compare the proposed and the non-robust approaches in terms of the MSE. We also consider two benchmarks with perfect CSI, namely the proposed approach and the AF O-Ps scheme. It can be observed that the non-robust approach leads to the worst system performance, i.e., the highest MSE, whereas the proposed solution for imperfect CSI outperforms the non-robust approach (especially for low SNR values), and comes close to the considered benchmarks.

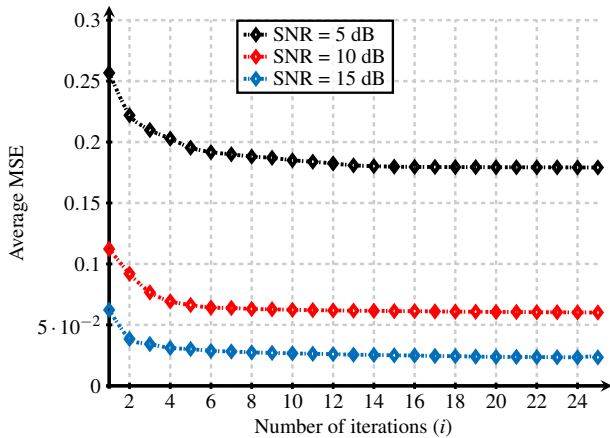


Fig. 10. Average MSE vs number of iterations ( $i$ ) for  $K = 3$  users,  $N_t = 4$ ,  $N_f = 9$ ,  $N = 25$ ,  $\text{SNR (dB)} \in \{5, 10, 15\}$ ,  $L = 32$  imperfect CSI, and  $N_{s,k}[\ell] = 2, \forall k, \ell$ .

In the last experiment, we empirically evaluate the convergence of Algorithm 1. Specifically, Fig. 10 illustrates the evolution of the average MSE (sum MSE divided by  $K = 3$  users) concerning the number of iterations performed in the alternating procedure. We considered three different SNR levels, namely  $\text{SNR (dB)} \in \{5, 10, 15\}$ . Note that convergence is achieved after 25 iterations in all cases. As mentioned in Section V, proving global optimality for the algorithm is challenging. However, in our simulations, we have observed that the algorithm converges rapidly within the first few iterations.

The conducted simulations reveal several remarkable results, which are summarized below:

- 1) The proposed PG-based approach outperforms the random configuration of the IRS-phase shift matrix, approaching the system capacity (Fig. 4).
- 2) *The key is in the phase changes.* The proper configuration of our passive IRS does not lead to a big gap w.r.t. the approach where phases and amplitudes are properly changed in an active (power-limited) IRS, in the strategy termed as AF O-Ps (Fig. 4).

- 3) *The placement of the IRS is crucial.* The gains provided by the IRS become lower when the IRS-user links become worse, i.e., the enhancement provided by the IRS is conditioned to the rank of the IRS-user channels (Table VI).
- 4) The use of low bit-resolution discrete phase shifts at the IRS is effective in achieving a substantial system sum rate that is comparable to the ideal scenario with continuous phase shifts (Fig. 5 and Fig. 6).
- 5) The performance gain achieved by the proposed solution over an IRS with random phase shifts saturates with a large number of IRS elements, depending on the wideband ( $L$  subcarriers)  $K$ -users-MIMO setup (Fig. 7).
- 6) The proposed solution in Algorithm 1 is robust for imperfect CSI as it incorporates the statistics of channel estimation errors and achieves a substantial gain over a non-robust strategy (Fig. 8 and Fig. 9). Additionally, the developed approach is independent to the modeling of the statistics of the errors.

## VIII. CONCLUSIONS

The design of an IRS-aided wideband MU MIMO system under imperfect CSI has been addressed in this paper. An innovative alternating minimization algorithm has been proposed to configure the frequency-flat IRS phase-shift matrix as well as the wideband BS precoders and user filters. The algorithm minimizes the MSE between the symbols sent by the users and those received at the BS in the dual MAC. Imperfect CSI is assumed and the available information on CSI errors statistics is incorporated into the system design. The results show reasonable gains in terms of both the achievable rate and the MSE over baseline strategies. Specifically, the deployment of the IRS and the adequate configuration of the phase shift matrix provides significant performance gains with respect to non-IRS conventional systems with MRT precoding.

## ACKNOWLEDGMENTS

This work has been supported by grants PID2019-104958RB-C42 (ADELE), PID2022-137099NB-C42 (MADDIE), and BES-2017-081955 funded by MCIN/AEI/10.13039/501100011033. José P. González-Coma thanks the Defense University Center at the Spanish Naval Academy for all the support provided for this research.

## REFERENCES

- [1] Y.-C. Liang, R. Long, Q. Zhang, J. Chen, H. V. Cheng, and H. Guo, "Large intelligent surface/antennas (LISA): Making reflective radios smart," *J. Commun. Net.*, vol. 4, no. 2, pp. 40–50, 2019.
- [2] Q. Wu, S. Zhang, B. Zheng, C. You, and R. Zhang, "Intelligent reflecting surface-aided wireless communications: A tutorial," *IEEE Trans. Commun.*, vol. 69, no. 5, pp. 3313–3351, 2021.
- [3] Ö. Özdoğan, E. Björnson, and E. G. Larsson, "Intelligent reflecting surfaces: Physics, propagation, and pathloss modeling," *IEEE Wireless Commun. Lett.*, vol. 9, no. 5, pp. 581–585, 2020.

- [4] E. Basar, M. Di Renzo, J. De Rosny, M. Debbah, M.-S. Alouini, and R. Zhang, “Wireless communications through reconfigurable intelligent surfaces,” *IEEE Access*, vol. 7, pp. 116 753–116 773, 2019.
- [5] S. Gong, X. Lu, D. T. Hoang, D. Niyato, L. Shu, D. I. Kim, and Y.-C. Liang, “Toward smart wireless communications via intelligent reflecting surfaces: A contemporary survey,” *IEEE Commun. Surv. Tutor.*, vol. 22, no. 4, pp. 2283–2314, 2020.
- [6] H. Gacanin and M. Di Renzo, “Wireless 2.0: Toward an intelligent radio environment empowered by reconfigurable meta-surfaces and artificial intelligence,” *IEEE Veh. Technol. Mag.*, vol. 15, no. 4, pp. 74–82, 2020.
- [7] F. Boccardi, R. W. Heath, A. Lozano, T. L. Marzetta, and P. Popovski, “Five disruptive technology directions for 5G,” *IEEE Commun. Mag.*, vol. 52, no. 2, pp. 74–80, 2014.
- [8] T. S. Rappaport, R. W. Heath, R. C. Daniels, and J. N. Murdock, “Millimeter Wave Wireless Communications,” *Prentice-Hall*, September, 2014.
- [9] R. W. Heath, N. González-Prelcic, S. Rangan, W. Roh, and A. M. Sayeed, “An overview of signal processing techniques for millimeter wave MIMO systems,” *IEEE J. Sel. Top. Signal Process.*, vol. 10, no. 3, pp. 436–453, 2016.
- [10] S. Rangan, T. S. Rappaport, and E. Erkip, “Millimeter-wave cellular wireless networks: Potentials and challenges,” *Proc. IEEE*, vol. 102, no. 3, pp. 366–385, 2014.
- [11] J. G. Andrews, S. Buzzi, W. Choi, S. V. Hanly, A. Lozano, A. C. K. Soong, and J. C. Zhang, “What will 5g be?” *IEEE J. Sel. Areas Commun.*, vol. 32, no. 6, pp. 1065–1082, 2014.
- [12] D. Pérez-Adán, Ó. Fresnedo, J. P. Gonzalez-Coma, and L. Castedo, “Intelligent reflective surfaces for wireless networks: An overview of applications, approached issues, and open problems,” *Electronics*, vol. 10, no. 19, p. 2345, 2021.
- [13] H. A. U. Mustafa, M. A. Imran, M. Z. Shakir, A. Imran, and R. Tafazolli, “Separation framework: An enabler for cooperative and D2D communication for future 5G networks,” *IEEE Commun. Surv. Tutor.*, vol. 18, no. 1, pp. 419–445, 2016.
- [14] J. Yuan, Y.-C. Liang, J. Joung, G. Feng, and E. G. Larsson, “Intelligent reflecting surface-assisted cognitive radio system,” *IEEE Trans. Commun.*, vol. 69, no. 1, pp. 675–687, 2021.
- [15] R. Allu, O. Taghizadeh, S. K. Singh, K. Singh, and C.-P. Li, “Robust beamformer design in active RIS-assisted multiuser MIMO cognitive radio networks,” *IEEE Trans. Cogn. Commun. Netw.*, vol. 9, no. 2, pp. 398–413, 2023.
- [16] Z. Ding and H. Vincent Poor, “A simple design of IRS-NOMA transmission,” *IEEE Commun. Lett.*, vol. 24, no. 5, pp. 1119–1123, 2020.
- [17] X. Guo, Y. Chen, and Y. Wang, “Learning-based robust and secure transmission for reconfigurable intelligent surface aided millimeter wave UAV communications,” *IEEE Wirel. Commun. Lett.*, vol. 10, no. 8, pp. 1795–1799, 2021.
- [18] E. Björnson, Ö. Özdogan, and E. G. Larsson, “Intelligent reflecting surface versus decode-and-forward: How large surfaces are needed to beat relaying?” *IEEE Wireless Commun. Lett.*, vol. 9, no. 2, pp. 244–248, 2020.
- [19] Ö. Özdogan, E. Björnson, and E. G. Larsson, “Using intelligent reflecting surfaces for rank improvement in MIMO communications,” in *Proc. of the IEEE Int. Conf. Acoust., Speech Signal Process. (ICASSP)*, 2020, pp. 9160–9164.
- [20] M. Jung, W. Saad, M. Debbah, and C. S. Hong, “Asymptotic optimality of reconfigurable intelligent surfaces: Passive beamforming and achievable rate,” in *Proc. of the IEEE Int. Conf. Commun. (ICC)*, 2020, pp. 1–6.
- [21] S. Hu, Z. Wei, Y. Cai, C. Liu, D. W. K. Ng, and J. Yuan, “Robust and secure sum-rate maximization for multiuser MISO downlink systems with self-sustainable IRS,” *IEEE Trans. Commun.*, vol. 69, no. 10, pp. 7032–7049, 2021.
- [22] M. Fu, Y. Zhou, and Y. Shi, “Intelligent reflecting surface for downlink non-orthogonal multiple access networks,” in *Proc. of the IEEE Glob. Commun. Conf. (GLOBECOM)*, Dec. 2019, pp. 1–6.
- [23] W. Yan, X. Yuan, Z.-Q. He, and X. Kuai, “Passive beamforming and information transfer design for reconfigurable intelligent surfaces aided multiuser MIMO systems,” *IEEE J. Sel. Areas Commun.*, vol. 38, no. 8, pp. 1793–1808, 2020.
- [24] D. Pereira-Ruisanchez, O. Fresnedo, D. Perez-Adan, and L. Castedo, “Deep contextual bandit and reinforcement learning for IRS-assisted MU-MIMO systems,” *IEEE Trans. Veh. Technol.*, vol. 72, no. 7, pp. 9099–9114, 2023.
- [25] M. Yue, L. Liu, and X. Yuan, “RIS-aided multiuser MIMO-OFDM with linear precoding and iterative detection: Analysis and optimization,” *IEEE Trans. Wirel. Commun.*, 2023.
- [26] H. Schulze and C. Lüders, *Theory and applications of OFDM and CDMA: Wideband wireless communications*. John Wiley & Sons, 2005.
- [27] J. Zhang, Y. Zhang, C. Zhong, and Z. Zhang, “Robust design for intelligent reflecting surfaces assisted MISO systems,” *IEEE Commun. Lett.*, vol. 24, no. 10, pp. 2353–2357, 2020.
- [28] G. Zhou, C. Pan, H. Ren, K. Wang, M. D. Renzo, and A. Nallanathan, “Robust beamforming design for intelligent reflecting surface aided MISO communication systems,” *IEEE Wireless Commun. Lett.*, vol. 9, no. 10, pp. 1658–1662, 2020.
- [29] M.-M. Zhao, Q. Wu, M.-J. Zhao, and R. Zhang, “IRS-aided wireless communication with imperfect CSI: Is amplitude control helpful or not?” in *IEEE Glob. Commun. Conf.*, 2020, pp. 1–6.
- [30] G. Zhou, C. Pan, H. Ren, K. Wang, and A. Nallanathan, “A framework of robust transmission design for IRS-aided MISO communications with imperfect cascaded channels,” *IEEE Trans. Signal Process.*, vol. 68, pp. 5092–5106, 2020.



- [31] M.-M. Zhao, Q. Wu, M.-J. Zhao, and R. Zhang, "Exploiting amplitude control in intelligent reflecting surface aided wireless communication with imperfect CSI," *IEEE Trans. Commun.*, vol. 69, no. 6, pp. 4216–4231, 2021.
- [32] Y. Chen, Y. Wang, Z. Wang, and P. Zhang, "Robust beamforming for active reconfigurable intelligent omni-surface in vehicular communications," *IEEE J. Sel. Areas Commun.*, vol. 40, no. 10, pp. 3086–3103, 2022.
- [33] J. P. González-Coma, J. Rodríguez-Fernández, N. González-Prelcic, L. Castedo, and R. W. Heath, "Channel estimation and hybrid precoding for frequency selective multiuser mmWave MIMO systems," *IEEE J. Sel. Top. Signal Process.*, vol. 12, no. 2, pp. 353–367, 2018.
- [34] D. Pérez-Adán, O. Fresnedo, J. P. González-Coma, and L. Castedo, "Wideband user grouping for uplink multiuser mmWave MIMO systems with hybrid combining," *IEEE Access*, vol. 9, pp. 41 360–41 372, 2021.
- [35] P. Wang, J. Fang, H. Duan, and H. Li, "Compressed channel estimation for intelligent reflecting surface-assisted millimeter wave systems," *IEEE Signal Process. Lett.*, vol. 27, pp. 905–909, 2020.
- [36] M. Joham, H. Gao, and W. Utschick, "Estimation of channels in systems with intelligent reflecting surfaces," in *Proc. of IEEE Int. Conf. Acoust., Speech Signal Process. (ICASSP)*. IEEE, 2022, pp. 5368–5372.
- [37] J. Brewer, "Kronecker products and matrix calculus in system theory," *IEEE Trans. Circuits Syst.*, vol. 25, no. 9, pp. 772–781, 1978.
- [38] M. Joham, P. M. Castro, W. Utschick, and L. Castedo, "Robust precoding with limited feedback design based on precoding MSE for MU-MISO systems," *IEEE Trans. Signal Process.*, vol. 60, no. 6, pp. 3101–3111, 2012.
- [39] M. Joham, P. M. Castro, L. Castedo, and W. Utschick, "Robust precoding with bayesian error modeling for limited feedback MU-MISO systems," *IEEE Trans. Signal Process.*, vol. 58, no. 9, pp. 4954–4960, 2010.
- [40] A. Sayeed, "Deconstructing multiantenna fading channels," *IEEE Trans. Signal Process.*, vol. 50, no. 10, pp. 2563–2579, 2002.
- [41] P. Schniter and A. Sayeed, "Channel estimation and precoder design for millimeter-wave communications: The sparse way," in *2014 48th Asilomar Conf. Signals Syst. Comput.*, 2014, pp. 273–277.
- [42] C. A. Balanis, *Antenna theory: analysis and design*. John Wiley & sons, 2015.
- [43] J. P. González-Coma, M. Joham, P. M. Castro, and L. Castedo, "QoS constrained power minimization in the multiple stream MIMO broadcast channel," *Signal Process.*, vol. 143, pp. 48–55, 2018.
- [44] R. Hunger, M. Joham, and W. Utschick, "On the MSE-duality of the broadcast channel and the multiple access channel," *IEEE Trans. Signal Process.*, vol. 57, no. 2, pp. 698–713, 2009.
- [45] S. S. Christensen, R. Agarwal, E. De Carvalho, and J. M. Cioffi, "Weighted sum-rate maximization using weighted MMSE for MIMO-BC beamforming design," *IEEE Trans. Wirel. Commun.*, vol. 7, no. 12, pp. 4792–4799, 2008.
- [46] T. Endeshaw, B. K. Chalise, and L. Vandendorpe, "MSE uplink-downlink duality of MIMO systems under imperfect CSI," in *Proc. of 3rd IEEE Int. Work. on Comp. Adv. in Multi-Sensor Adapt. Process. (CAMSAP)*. IEEE, 2009, pp. 384–387.
- [47] M. Joham, M. Vonbun, and W. Utschick, "MIMO BC/MAC MSE duality with imperfect transmitter and perfect receiver CSI," in *Proc. of the IEEE Int. Work. Sig. Process. Adv. Wirel. Commun. (SPAWC)*, 2010, pp. 1–5.
- [48] S. Shi, M. Schubert, and H. Boche, "Downlink mmse transceiver optimization for multiuser MIMO systems: Duality and sum-MSE minimization," *IEEE Trans. Signal Process.*, vol. 55, no. 11, pp. 5436–5446, 2007.
- [49] D. P. Bertsekas, "On the Goldstein-Levitin-Polyak gradient projection method," *IEEE Trans. Autom. Control.*, vol. 21, no. 2, pp. 174–184, 1976.
- [50] P.-A. Absil, R. Mahony, and R. Sepulchre, *Optimization algorithms on matrix manifolds*. Princeton University Press, 2009.
- [51] J. M. Lee, "Smooth manifolds," in *Introduction to Smooth Manifolds*. Springer, 2013, pp. 1–31.
- [52] Y. Ma, Y. Shen, X. Yu, J. Zhang, S. Song, and K. B. Letaief, "A low-complexity algorithmic framework for large-scale IRS-assisted wireless systems," in *Proc. of the IEEE Glob. Work.*, 2020, pp. 1–6.
- [53] Y. Yang, M. Pesavento, Z.-Q. Luo, and B. Ottersten, "Inexact block coordinate descent algorithms for nonsmooth nonconvex optimization," *IEEE Trans. Signal Process.*, vol. 68, pp. 947–961, 2019.
- [54] J. C. Bezdek and R. J. Hathaway, "Convergence of alternating optimization," *Neural, Parallel & Scientific Computations*, vol. 11, no. 4, pp. 351–368, 2003.
- [55] J. P. González-Coma, W. Utschick, and L. Castedo, "Hybrid LISA for wideband multiuser millimeter-wave communication systems under beam squint," *IEEE Trans. Wirel. Commun.*, vol. 18, no. 2, pp. 1277–1288, 2019.
- [56] K. P. Rajput, P. Maity, S. Srivastava, V. Sharma, N. K. D. Venkatesowda, A. K. Jagannatham, and L. Hanzo, "Robust linear hybrid beamforming designs relying on imperfect CSI in mmWave MIMO IoT networks," *IEEE Internet Things J.*, vol. 10, no. 10, pp. 8893–8906, 2023.
- [57] Y. Rong, "Robust design for linear non-regenerative MIMO relays with imperfect channel state information," *IEEE Trans. Signal Process.*, vol. 59, no. 5, pp. 2455–2460, 2011.
- [58] N. Jindal, W. Rhee, S. Vishwanath, S. Jafar, and A. Goldsmith, "Sum power iterative water-filling for multi-antenna gaussian broadcast channels," *IEEE Trans. Inf. Theory*, vol. 51, no. 4, pp. 1570–1580, 2005.
- [59] D. Pérez-Adán, O. Fresnedo, J. P. González-Coma, and L. Castedo, "Alternating minimization algorithm for multiuser RIS-assisted MIMO systems," in *Proc. of the IEEE Int. Symp. Broadband Multimed. Syst. Broadcast. (BMSB)*, 2022, pp. 1–6.